Two-loop planar corrections to heavy-quark pair production in the quark-antiquark channel

Bonciani, R ; Ferroglia, A ; Gehrmann, T ; Studerus, C

Abstract: We evaluate the planar two-loop QCD diagrams contributing to the leading color coefficient of the heavy-quark pair production cross section, in the quark-antiquark annihilation channel. We obtain the leading color coefficient in an analytic form, in terms of one- and two-dimensional harmonic polylogarithms of maximal weight 4. The result is valid for arbitrary values of the Mandelstam invariants s and t, and of the heavy-quark mass m. Our findings agree with previous analytic results in the small-mass limit and numerical results for the exact amplitude.

DOI: https://doi.org/10.1088/1126-6708/2009/08/067

LPSC 09/73
MZ-TH/09-19
ZU-TH 11/09

Two-Loop Planar Corrections to Heavy-Quark Pair Production in the Quark-Antiquark Channel

R. Bonciani [a,*], **A. Ferroglia** [b,†], **T. Gehrmann** [c,‡] **and C. Studerus** [c,§]

[a] *Laboratoire de Physique Subatomique et de Cosmologie, Université Joseph Fourier/CNRS-IN2P3/INPG, F-38026 Grenoble, France*

[b] *Institut für Physik (THEP), Johannes Gutenberg-Universität, D-55099 Mainz, Germany*

[c] *Institut für Theoretische Physik, Universität Zürich, CH-8057 Zurich, Switzerland*

Abstract: We evaluate the planar two-loop QCD diagrams contributing to the heavy-quark pair production process in the quark-antiquark annihilation channel. The evaluation of these diagrams allows us to obtain an analytic expression for the leading color coefficient in the virtual corrections at order α_S^2. We obtain a result which is valid for any value of the Mandelstam invariants s and t, and of the heavy-quark mass m. Our findings agree with previous analytic results in the small-mass limit and numerical results for the exact amplitude.

Keywords: Heavy Quark Production, Two Loop Calculation.

*Email: bonciani@lpsc.in2p3.fr
†Email: ferroglia@thep.physik.uni-mainz.de
‡Email: Thomas.Gehrmann@physik.uzh.ch
§Email: cedric@physik.uzh.ch

Contents

1. Introduction

The top quark, with a mass of approximately 173 GeV, is the heaviest elementary particle produced at colliders until now. So far, the study of the properties of the top-quark was only possible at the Tevatron, where the mass of this particle was measured with an accuracy of less than one percent. The production cross sections and decay widths are only known with larger uncertainties. Because of its large mass, the top quark is expected to couple strongly with the electroweak symmetry breaking sector. Therefore, the study of scattering and decay processes involving top quarks is expected to provide fundamental clues on the mechanism responsible for the origin of particle masses. This is one of the main goals of the Large Hadron Collider (LHC) physics program.

While the Tevatron produced a few thousand top quarks, the LHC will be an authentic top-quark factory, since it will produce millions of top quarks already in the first low-luminosity phase [1]. The great wealth of data that will be obtained at the LHC will allow precise measurements of the top-quark related observables. In turn, the latter must be matched by equally precise calculations of the relevant cross sections and differential distributions in perturbative QCD.

At Tevatron, top quarks are primarily produced in pairs with their antiparticles. The same situation will be encountered at the LHC, where experimental collaborations anticipate measurements of the total top-quark pair-production cross section with a relative

error between 5% and 10%. On the theory side, the top-quark pair-production cross section was calculated at next-to-leading-order (NLO) in perturbative QCD [2–9]. The NLO electroweak corrections were obtained in [10–12]. The resummation of logarithmic terms, which become large near the production threshold, was extensively studied in [13–19].

The current resummation-improved NLO predictions for the top-quark pair-production cross section at the LHC shows an uncertainty of about 15% [1]; the latter is dominated by the scale uncertainty. Therefore, in order to reduce the theoretical uncertainty at the same level of the expected experimental error, the calculation of the next-to-next-to-leading order (NNLO) perturbative QCD corrections is required.

The Feynman diagrams needed for the evaluation of the NNLO QCD corrections to the top-quark pair production can be grouped in three categories: i) two-loop corrections to the three-level production channels $q\bar{q} \to t\bar{t}$ and $gg \to t\bar{t}$, ii) one-loop matrix elements with an additional parton in the final state, and iii) tree-level matrix element with two additional partons in the final state. The last two sets of diagrams were already evaluated in the context of the calculation of the NLO corrections to the production of $t\bar{t} + 1j$ [20]. Contributions arising from the interference of one-loop diagrams in both the quark-antiquark and the gluon-fusion channels were studied in [21–24]. The first steps toward the calculation of the two-loop corrections were taken in [25, 26]; in these papers all the relevant two-loop diagrams were evaluated in the limit $s, |t|, |u| \gg m^2$, where s is the squared center of mass energy, t is the squared momentum transfer, $u = 2m^2 - s - t$ and m is the heavy-quark mass. A full numerical calculation of the two-loop virtual corrections in the $q\bar{q} \to t\bar{t}$ channel was carried out in [27]. Finally, the analytic calculation of the diagrams involving a closed quark loop in the quark-antiquark channel was presented in [28].

In this paper we describe the calculation of the two-loop planar diagrams in the $q\bar{q} \to t\bar{t}$ production channel. The calculation of this subset of corrections allows us to obtain an analytic expression for the leading color coefficient in the interference of the two-loop matrix element with the tree-level amplitude. Our results are valid for generic values of the Mandelstam invariants s, t and of the heavy-quark mass m. The calculation was carried out by means of a technique based on the identification of a set of Master Integrals (MIs) through the Laporta algorithm [29], and on their subsequent evaluation by means of the differential equation method [30]. The results are written in terms of a suitable base of one- and two-dimensional Harmonic Polylogarithms (HPLs) [31–33].

The paper is organized as follows. In Section 2 we introduce our notation and conventions. In Section 3 the method employed in the calculation is briefly described and the technical difficulties we met are discussed. In Section 4 we collect the explicit expression of the counterterms needed for the ultraviolet renormalization of the Feynman diagrams which we evaluated. The results which we obtained and their expansion near the production threshold are discussed in Section 5. Section 6 contains our conclusions. In the appendices we describe in some detail the HPLs we employed in the calculation and their expansion at production threshold. Furthermore, we collect the explicit expression of several previously unknown MIs belonging to box topologies.

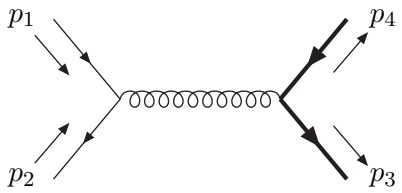

Figure 1: *Tree-level amplitude. Massive quarks are indicated by a thick line.*

2. Notation and Conventions

We consider the scattering process

$$q(p_1) + \overline{q}(p_2) \longrightarrow t(p_3) + \overline{t}(p_4)\,, \tag{2.1}$$

in Euclidean kinematics, where $p_i^2 = 0$ for $i = 1, 2$ and $p_j^2 = -m^2$ for $j = 3, 4$. The Mandelstam variables are defined as follows

$$s = -\left(p_1 + p_2\right)^2\,, \quad t = -\left(p_1 - p_3\right)^2\,, \quad u = -\left(p_1 - p_4\right)^2\,. \tag{2.2}$$

Conservation of momentum implies that $s + t + u = 2m^2$.

The squared matrix element (averaged over the spin and color of the incoming quarks and summed over the spin of the outgoing ones), calculated in $d = 4 - 2\varepsilon$ dimensions, can be expanded in powers of the strong coupling constant α_S as follows:

$$|\mathcal{M}|^2(s,t,m,\varepsilon) = \frac{4\pi^2\alpha_S^2}{N_c^2}\left[\mathcal{A}_0 + \left(\frac{\alpha_S}{\pi}\right)\mathcal{A}_1 + \left(\frac{\alpha_S}{\pi}\right)^2\mathcal{A}_2 + \mathcal{O}\left(\alpha_S^3\right)\right]\,. \tag{2.3}$$

The tree-level amplitude involves a single diagram (Fig. 1) and its contribution to Eq. (2.3) is given by

$$\mathcal{A}_0 = 4N_c\,C_F\left[\frac{(t-m^2)^2 + (u-m^2)^2}{s^2} + \frac{2m^2}{s} - \varepsilon\right]\,, \tag{2.4}$$

where N_c is the number of colors and $C_F = (N_c^2 - 1)/2N_c$.

The $\mathcal{O}(\alpha_S)$ term $\mathcal{A}_1$ in Eq. (2.3) arises from the interference of one-loop diagrams with the tree-level amplitude [2–8]. The $\mathcal{O}(\alpha_S^2)$ term $\mathcal{A}_2$ consists of two parts, the interference of two-loop diagrams with the Born amplitude and the interference of one-loop diagrams among themselves:

$$\mathcal{A}_2 = \mathcal{A}_2^{(2\times0)} + \mathcal{A}_2^{(1\times1)}\,.$$

The latter term $\mathcal{A}_2^{(1\times1)}$ was studied extensively in [21, 22]. $\mathcal{A}_2^{(2\times0)}$, originating from the two-loop diagrams, can be decomposed according to color and flavor structures as follows:

$$\begin{aligned}\mathcal{A}_2^{(2\times0)} = N_c C_F\Bigg[&N_c^2 A + B + \frac{C}{N_c^2} + N_l\left(N_c D_l + \frac{E_l}{N_c}\right) + N_h\left(N_c D_h + \frac{E_h}{N_c}\right)\\ &+ N_l^2 F_l + N_l N_h F_{lh} + N_h^2 F_h\Bigg]\,,\end{aligned} \tag{2.5}$$

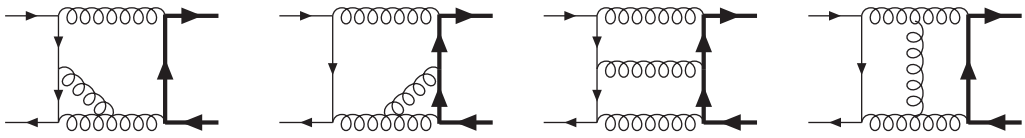

Figure 2: *Some of the two-loop planar box diagrams involved in the calculation.*

where N_l and N_h are the number of light- and heavy-quark flavors, respectively. The coefficients $A, B, \ldots, F_h$ in Eq. (2.5) are functions of s, t, and m, as well as of the dimensional regulator ε. These quantities were calculated in [25] in the approximation $s, |t|, |u| \gg m^2$. For a fully differential description of top quark pair production at NNLO, the complete mass dependence of $\mathcal{A}_2^{(2\times 0)}$ is required. An exact numerical expression for it has been obtained in [27]. Exact analytic formulae for all the coefficients arising from Feynman diagrams involving closed quark loops ($D_l, E_l, D_h, E_h, F_l, F_h, F_{lh}$) were obtained in [28]. In this work, we provide an exact analytic expression for the coefficient A in Eq. (2.5), which arises from planar Feynman diagrams only.

3. Calculation

The package QGRAF [34] generates 218 two-loop Feynman diagrams contributing to the process $q\bar{q} \to t\bar{t}$. After treating the QGRAF output with FORM [35] in order to carry out the color (and Dirac) algebra, one finds that there are 44 non-vanishing diagrams contributing to the leading color coefficient in Eq. (2.5). Some of the box diagrams involved in the calculation are shown in Fig. 2. All the two-loop graphs encountered in our calculation can be treated by employing the technique based upon the Laporta algorithm for the reduction to a set of Master Integrals (MIs). The MIs are then evaluated by means of the differential equation method.

A subset of the MIs needed in the calculation were available in the literature [36–41]. They were employed in previous two-loop calculations of the heavy-quark form factors [42], amplitudes for Bhabha scattering [43], heavy-to-light quark transitions [44], and in the calculation of the fermionic corrections to $q\bar{q} \to t\bar{t}$ [28]. The MIs not included in this subset are a part of the original findings of this paper.

The reduction to MIs was carried out with an implementation of the Laporta algorithm written in `C++` [45], and large parts of it were cross checked with the `Maple` package `A.I.R.` [46]. The six so far unknown irreducible topologies encountered in the calculation of the planar diagrams are shown in Fig. 3. In the figure, thick internal lines indicate massive propagators, while thin lines indicate massless ones. An external dashed leg carries a squared momentum $(p_1 + p_2)^2 = -s$; other external lines indicate particles on their mass-shell, where $p_i^2 = 0$ for thin lines and $p_i^2 = -m^2$ for thick lines. The MIs in Fig. 3 are collected in Appendix C and in a file included with the arXiv submission of the present paper.

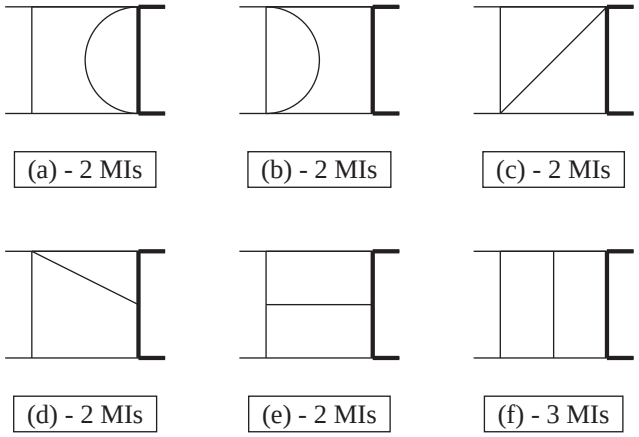

Figure 3: *New non-reducible topologies encountered in the calculation of the planar diagrams. The number of Master Integrals related to each topology is indicated in the figure.*

In calculating the MIs by means of the differential equation method, it is crucial to fix the undetermined integration constant(s) through a boundary condition. While there is no general method available to fix this boundary condition, it is usually sufficient to know the behavior of the MI at some particular kinematic point. For example, knowing that the integral is regular for a certain value of s, one can impose the regularity of the solution of the differential equation at that point. In cases in which considerations related to the regularity of the solutions of the differential equations are not sufficient to fix all of the integration constants, it is necessary to directly evaluate the MIs at a specific phase-space point. This can be done using techniques based on Mellin-Barnes representations of the integrals [47], with the help of the `Mathematica` packages `Ambre` [48] and `MB` [49]. In order to numerically check the analytic calculation of the MIs, we employed the sector decomposition technique [50], implemented in the `Mathematica` package `FIESTA` [51].

All the MIs were calculated in the non-physical region $s < 0$, where they are real and can be conveniently written as functions of the dimensionless variables

$$x = \frac{\sqrt{-s+4m^2} - \sqrt{-s}}{\sqrt{-s+4m^2} + \sqrt{-s}}\,, \qquad y = \frac{-t}{m^2}\,. \tag{3.1}$$

The transcendental functions appearing in the results are one- and two-dimensional harmonic polylogarithms (HPLs) [31–33, 40] of maximum weight four. In Appendix A, we briefly review the definition of the HPLs appearing in the calculation. All the HPLs appearing in the analytic expression of the coefficient A can be evaluated numerically with arbitrary precision by employing the methods and codes described in [32].

Following the procedure outlined in the present section, it is possible to obtain the expression of the bare squared matrix elements involving planar two-loop diagrams. The renormalization of the ultraviolet divergencies is discussed in the next section.

4. Renormalization

The renormalized QCD matrix element is obtained from the bare one by expanding the following expression :

$$\mathcal{A}_{\rm ren} = \prod_n Z_{{\rm WF},n}^{1/2}\, \mathcal{A}_{\rm bare}\left(\alpha_{S,{\rm bare}} \to Z_{\alpha_S}\alpha_S\,, m_{\rm bare} \to Z_m m\right)\,, \tag{4.1}$$

where $Z_{{\rm WF},n}$ is the external leg wave function renormalization factor, α_S is the renormalized coupling constant and m is the renormalized heavy-quark mass. (In the rest of the section we suppress the subscript "S" in α_S).

We postpone the discussion of mass renormalization to the end of the section and we start by considering the coupling constant and wave function renormalization.

We introduce the following quantities:

$$a_0 = \frac{\alpha_{\rm bare}}{\pi}\,, \qquad \text{and} \qquad a = \frac{\alpha}{\pi}\,. \tag{4.2}$$

By expanding the amplitude and the wave function renormalization factor in a_0 we find:

$$\begin{aligned} \mathcal{A}_{\rm ren}(\alpha_{\rm bare}) &= a_0\mathcal{A}_0 + a_0^2\mathcal{A}_1 + a_0^3\mathcal{A}_2 + \mathcal{O}(a_0^4)\,, \\ Z_{{\rm WF},n} &= 1 + a_0\delta Z_{{\rm WF},n}^{(1)} + a_0^2\delta Z_{{\rm WF},n}^{(2)} + \mathcal{O}(a_0^3)\,. \end{aligned} \tag{4.3}$$

The relation between a_0 and a is given by:

$$a_0 = a + a^2\delta Z_\alpha^{(1)} + a^3\delta Z_\alpha^{(2)} + \mathcal{O}(a^4)\,. \tag{4.4}$$

By employing Eqs. (4.3,4.4) in Eq. (4.1) we find

$$\begin{aligned} \mathcal{A}_{\rm ren} &= a\mathcal{A}_0 + a^2\mathcal{A}_{\rm ren}^{(1)} + a^3\mathcal{A}_{\rm ren}^{(2)} + \mathcal{O}(a^4)\,, \\ \mathcal{A}_{\rm ren}^{(1)} &= \mathcal{A}_1 + \left(\sum_n \frac{1}{2}\delta Z_{{\rm WF},n}^{(1)} + \delta Z_\alpha^{(1)}\right)\mathcal{A}_0\,, \\ \mathcal{A}_{\rm ren}^{(2)} &= \mathcal{A}_2 + \left(\sum_n \frac{1}{2}\delta Z_{{\rm WF},n}^{(1)} + 2\delta Z_\alpha^{(1)}\right)\mathcal{A}_1 + \left(-\sum_n \frac{1}{8}\left(\delta Z_{{\rm WF},n}^{(1)}\right)^2\right. \\ &\quad \left. + \sum_n \frac{1}{2}\delta Z_{{\rm WF},n}^{(2)} + \delta Z_\alpha^{(1)}\sum_n \delta Z_{{\rm WF},n}^{(1)} + \delta Z_\alpha^{(2)}\right)\mathcal{A}_0\,. \end{aligned} \tag{4.5}$$

In the equations above, $\mathcal{A}_i$ represents the bare amplitude at i loops stripped of the factor a. In the case of the process $q\overline{q} \to t\overline{t}$, the wave function renormalization factors of massless quarks vanish at one loop, while the ones of the massive quarks in the on-shell renormalization scheme are given by

$$\delta Z_{{\rm WF},M}^{(1)} = C(\varepsilon)\left(\frac{\mu^2}{m^2}\right)^\varepsilon C_F\left(-\frac{3}{4\varepsilon} - \frac{1}{1-2\varepsilon}\right)\,, \tag{4.6}$$

where the subscript M indicates massive quarks and where $C(\varepsilon) = (4\pi)^\varepsilon\Gamma(1+\varepsilon)$. The one-loop renormalization constant for α in the $\overline{MS}$ scheme is given by

$$\delta Z_\alpha^{(1)} = C(\varepsilon)\,\frac{e^{-\gamma\varepsilon}}{\Gamma(1+\varepsilon)}\left(-\frac{\beta_0}{2\varepsilon}\right)\,, \tag{4.7}$$

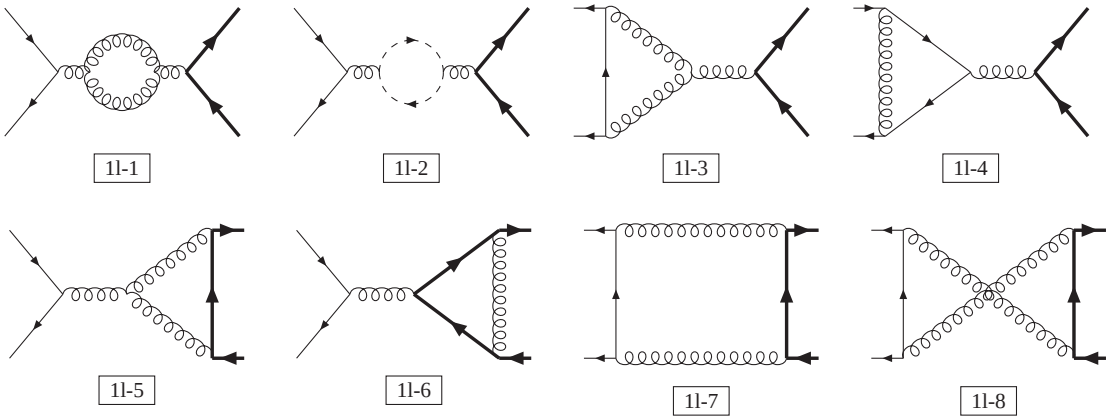

Figure 4: *One-loop diagrams (excluding the diagrams with closed quark loops). Thin arrow lines represent massless quarks, thick arrow line massive quarks, dashed arrow lines are Faddeev-Popov ghosts, and coiled lines are gluons.*

where $\beta_0 = 11/6C_A - 1/3(N_l + N_h)$ and γ is the Euler-Mascheroni constant $\gamma \approx 0.577216$.

Therefore, the overall one-loop counter term is given by

$$\delta Z^{(1)}_{\mathrm{WF},M} + \delta Z^{(1)}_{\alpha} = -\frac{C(\varepsilon)}{4\varepsilon}\left[2\beta_0 + \left(3 + 4\varepsilon + 3\varepsilon \ln\left(\frac{\mu^2}{m^2}\right)\right) C_F + \mathcal{O}\left(\varepsilon^2\right)\right] . \tag{4.8}$$

Here we are interested in finding the ultraviolet counterterm needed to renormalize the two-loop diagrams not involving closed quark loops. The part of this counterterm needed to renormalize the leading color structure in Eq. (2.5) can then be trivially extracted. Taking into account the fact that the wave function renormalization factors are zero for the incoming particles and identical for the massive ones, one finds that the renormalized amplitude (excluding quark-loop diagrams) is

$$\begin{aligned}\mathcal{A}^{(2,\mathrm{g})}_{\mathrm{ren}} = \mathcal{A}^{(\mathrm{g})}_2 + \left(\delta Z^{(1)}_{\mathrm{WF},M} + 2\delta Z^{(1,C_A)}_{\alpha}\right) \sum_{j=1}^{8} \mathcal{A}^{(d_j)}_1 - \delta Z^{(1)}_m \sum_{l=5}^{8} \mathcal{A}^{(d_l,\texttt{mass ct})}_1 + \\ + \left(\delta Z^{(2,\mathrm{g})}_{\mathrm{WF},M} + 2\delta Z^{(1,C_A)}_{\alpha}\delta Z^{(1)}_{\mathrm{WF},M} + \delta Z^{(2,\mathrm{g})}_{\alpha}\right) \mathcal{A}_0 \,. \end{aligned} \tag{4.9}$$

In Eq. (4.9), the quantity $\mathcal{A}^{(d_j)}_1$ is the amplitude of the j-th diagram in Fig. 4 (stripped of the factor a). The quantity $\mathcal{A}^{(d_l,\texttt{mass ct})}$ indicates the l-th diagram in Fig. 4 with a mass counter term insertion in one of the internal heavy quark lines. The renormalization coefficients not previously defined are:

$$\begin{aligned}\delta Z^{(1)}_m &= \delta Z^{(1)}_{\mathrm{WF},M} \,, \\ \delta Z^{(1,C_A)}_{\alpha} &= -C(\varepsilon)\,\frac{e^{-\gamma\varepsilon}}{\Gamma(1+\varepsilon)}\,C_A \frac{11}{12\varepsilon} \,, \\ \delta Z^{(2,\mathrm{g})}_{\alpha} &= C(\varepsilon)^2 \left(\frac{e^{-\gamma\varepsilon}}{\Gamma(1+\varepsilon)}\right)^2 \frac{1}{4\varepsilon}\left[\left(\frac{11}{6}\right)^2 \frac{C_A^2}{\varepsilon} - \frac{17}{12} C_A^2\right] ,\end{aligned}$$

$$\delta Z^{(2,\mathrm{g})}_{\mathrm{WF},M} = C(\varepsilon)^2 \left(\frac{\mu^2}{m^2}\right)^{2\varepsilon} C_F \Bigg[C_F \left(\frac{9}{32\varepsilon^2} + \frac{51}{64\varepsilon} + \frac{433}{128} - \frac{3}{2}\zeta(3) + \pi^2 \ln 2 - \frac{13}{16}\pi^2 \right) + \\ + C_A \left(-\frac{11}{32\varepsilon^2} - \frac{101}{64\varepsilon} - \frac{803}{128} + \frac{3}{4}\zeta(3) - \frac{\pi^2}{2}\ln 2 + \frac{5}{16}\pi^2 \right) + \mathcal{O}(\varepsilon) \Bigg], \qquad (4.10)$$

and they can be found in [25, 52].

5. Results

The main result of the present paper is an analytic, non-approximated expression for the coefficient A in Eq. (2.5). Since such a result is too long to be explicitly printed here, we included in the arXiv submission of this work a text file with the complete result, which is written in terms of one- and two-dimensional HPLs of maximum weight four. Since the coefficients in Eq. (2.5) still contain infrared poles, the result is dependent on the choice of a global, ε-dependent normalization factor. With our choice, we factor out an overall coefficient

$$C^2(\varepsilon) = \left[(4\pi)^\varepsilon \, \Gamma(1+\varepsilon)\right]^2 . \qquad (5.1)$$

We also provide a code that numerically evaluates the analytic expression of the quantities listed above for arbitrary values of the mass scales involved in the calculation. The code is written in `C++` and uses the package for the evaluation of multiple polylogarithms within `GiNaC` [32].

In order to cross check our results, we expanded them in the $s, |t|, |u| \gg m^2$ limit. The first term in the expansion agrees with the results published in [25]; the second order term agrees with the results found in the `Mathematica` files included in the arXiv version of [27]. We also find complete agreement with the numerical result of Table 3 in [27], corresponding to a phase-space point in which the $s, |t|, |u| \gg m^2$ approximation cannot be applied. With our code it is also possible to reproduce the first plot in Figure 4 of [27], where the finite part of A is shown as a surface depending on the variables η and ϕ, defined as

$$\eta = \frac{s}{4m^2} - 1 , \quad \phi = -\frac{t-m^2}{s} , \quad \frac{1}{2}\left(1 - \sqrt{\frac{\eta}{1+\eta}}\right) \leq \phi \leq \frac{1}{2}\left(1 + \sqrt{\frac{\eta}{1+\eta}}\right) . \qquad (5.2)$$

This surface is shown on the left side of Figure 5.

Furthermore, it is possible to expand our result for values of the center of mass energy close to the production threshold. We define

$$\beta = \sqrt{1 - \frac{4m^2}{s}} , \qquad \xi = \frac{1-\cos\theta}{2} , \qquad L_\mu = \ln\left(\frac{\mu^2}{m^2}\right) , \qquad (5.3)$$

where θ is the scattering angle in the partonic center of mass frame, and we expand our results in powers of the heavy quark velocity β, up to terms of order β^2. The coefficients of this expansion contain transcendental constants which originate from one- and two-dimensional HPLs evaluated at $x = 1$. Since we did not find a satisfactory analytical representation for all of these constants, in the formulae below we present them in a

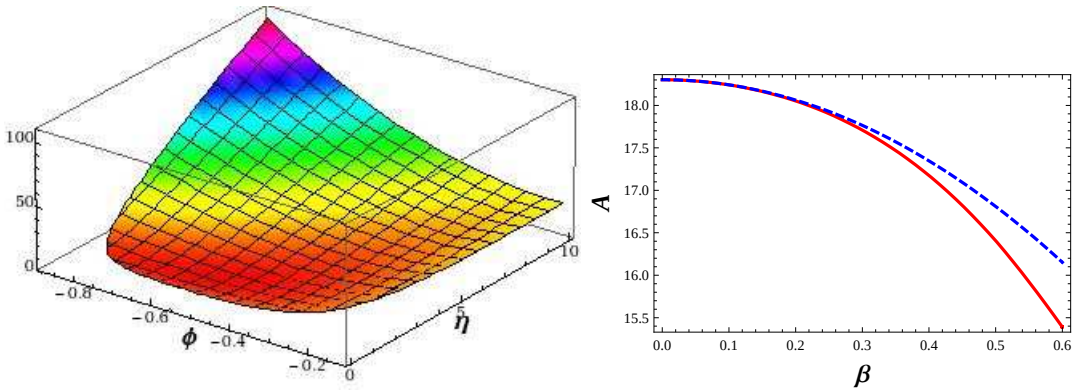

Figure 5: *Left: finite part of the coefficient A as a function of the variables η and ϕ. Right: the exact value of $A^{(0)}$ as a function of β (red solid curve) versus its expansion close to threshold up to terms of order β^2 (blue dashed curve). Both curves are plotted for $\xi = 1/2$. In both cases we used the normalization adopted in [27] to facilitate comparisons.*

numerical form. We find:

$$
\begin{aligned}
A(\beta,\xi) &= \frac{A^{(-4)}(\beta,\xi)}{\varepsilon^4} + \frac{A^{(-3)}(\beta,\xi)}{\varepsilon^3} + \frac{A^{(-2)}(\beta,\xi)}{\varepsilon^2} + \frac{A^{(-1)}(\beta,\xi)}{\varepsilon} + A^{(0)}(\beta,\xi) + \mathcal{O}(\varepsilon) \,, \\
A^{(-4)} &= 0.25 - 0.5\beta^2 (1-\xi)\,\xi + \mathcal{O}\left(\beta^3\right) \,, \\
A^{(-3)} &= 1.68185 + 0.5 L_\mu + \beta(1-2\xi) - \beta^2\Big[0.5 + \xi(1-\xi)(5.86371 + L_\mu)\Big] + \mathcal{O}\left(\beta^3\right) \,, \\
A^{(-2)} &= -2.67119 - 0.302961 L_\mu + 0.5 L_\mu^2 + \beta\Big[1.84475 + 2L_\mu - \xi(3.68951 + 4L_\mu)\Big] \\
&\quad + \beta^2\Big[0.777936 - L_\mu - \xi(1-\xi)(7.03784 + 4.39408 L_\mu + L_\mu^2)\Big] + \mathcal{O}\left(\beta^3\right) \,, \\
A^{(-1)} &= -8.15701 - 5.7593 L_\mu - 2.13629 L_\mu^2 + 0.333333 L_\mu^3 + \beta\Big[-9.83935 - 3.64382 L_\mu \\
&\quad + 2L_\mu^2 + \xi(19.6787 + 7.28765 L_\mu - 4L_\mu^2)\Big] + \beta^2\Big[2.78693 + 5.22254 L_\mu \\
&\quad - L_\mu^2 + \xi(1-\xi)(46.7006 + 8.75816 L_\mu - 0.727411 L_\mu^2 - 0.666667 L_\mu^3)\Big] + \mathcal{O}\left(\beta^3\right) \,, \\
A^{(0)} &= 23.5701 + 7.82592 L_\mu + 0.754463 L_\mu^2 - 2.03531 L_\mu^3 + 0.166667 L_\mu^4 + \\
&\quad \beta\Big[0.505501 - 11.5953 L_\mu - 7.31049 L_\mu^2 + 1.33333 L_\mu^3 + \xi(-1.011 + 23.1906 L_\mu \\
&\quad + 14.621 L_\mu^2 - 2.66667 L_\mu^3)\Big] + \beta^2\Big[-4.351 - 3.60348 L_\mu + 7.05587 L_\mu^2 \\
&\quad - 0.666667 L_\mu^3 + \xi(1-\xi)(-5.36823 + 43.1864 L_\mu + 6.73063 L_\mu^2 + 0.737281 L_\mu^3 \\
&\quad - 0.333333 L_\mu^4)\Big] + \mathcal{O}\left(\beta^3\right) \,.
\end{aligned}
\tag{5.4}
$$

Note that the dependence on β and on ξ in the formulae above is only polynomial. All the logarithmic terms $\ln\beta$, $\ln\xi$, $\ln(1-\xi)$, $\ln(1-2\,\xi)$, ..., which are indeed present in the expansion of individual HPLs, cancel out in the final expressions. The coefficient A is finite at threshold. The expansion presented here could be used in the future for the calculation of logarithmically enhanced terms near the $t\bar{t}$ production threshold. On the right hand side of Fig. 5, we compare the exact expression of the coefficient $A^{(0)}$ with the expansion

in powers of β including up to terms of order β^2 (in the plot we set $\xi = 1/2$).

6. Conclusions and Outlook

In this paper, we presented the analytic calculation of the two-loop planar corrections to the heavy-quark production amplitude for $q\bar{q} \to t\bar{t}$, retaining the exact heavy-quark mass dependence. The calculation of this subset of diagrams allowed us to obtain an analytic expression for the leading color coefficient in Eq. (2.5). We checked our formula against recent results obtained in analytic form in the small-mass region [25]. Moreover, we found numerical agreement with the value of A at the phase-space point presented in [27].

Our result represents a gauge invariant sub-set of the full two-loop corrections to the partonic process $q\overline{q} \to t\bar{t}$. In order to complete the analytic calculation of the two-loop corrections, it is necessary to calculate the non-planar diagrams. Likewise, analytic results for the two-loop amplitude for $gg \to t\bar{t}$ could be obtained in the same calculational framework [53]. However, some of the two-loop diagrams appearing in the gluon fusion channel cannot be expressed in terms of two-dimensional HPLs. In fact, their reduction to MIs involves a "sunrise"-type subtopology with three equal massive propagators and an external momentum which is not on the mass shell of the internal propagators. It is known that already such a three-propagator graph involves elliptic integrals [54].

In order to obtain NNLO predictions for the total $t\bar{t}$ production cross section and for differential distributions, it is necessary to combine the two-loop virtual corrections with the already available [20] one-loop corrections to the $t\bar{t}$+(1 parton) process and with the tree-level $t\bar{t}$+(2 partons) process. These diagrams with additional partons in the final state contribute to infrared-divergent configurations where up to two partons can become unresolved. Their implementation requires the application of a NNLO subtraction method. The methods presently available [50, 55, 56] have been applied up to now [57–60] to at most $1 \to 3$ processes in e^+e^- annihilation and $2 \to 1$ processes at hadron colliders. A calculation of a hadronic $2 \to 2$ process, involving massive partons, will represent a new step in complexity, potentially requiring further refinements of the methods available to date.

Acknowledgments

We would like to thank D. Maître for his help and suggestions and S. Weinzierl for useful discussions. This research was supported in part by the Theory-LHC-France initiative of CNRS/IN2P3, by the Swiss National Science Foundation (SNF) under contract 200020-117602, and by the "Forschungskredit der Universität Zürich".

A. Harmonic Polylogarithms

The results presented here are conveniently expressed in terms of one- and two-dimensional HPLs. Nowadays, harmonic polylogarithms are extensively employed in multiloop computations. Therefore, in this appendix we only briefly review their definition. The reader

interested in the algebraic properties of these functions can find detailed discussions about this topic in the available literature [31–33, 40].

In the non-physical region $s < 0$, seven weight functions are needed for the HPLs with argument x. They are[1]

$$f_w(x) = \frac{1}{x-w}\,, \quad \text{with} \quad w \in \left\{0, 1, -1, -y, -\frac{1}{y}, \frac{1}{2} \pm \frac{i\sqrt{3}}{2}\right\}\,. \tag{A.1}$$

For HPLs with argument y, we need six weight functions

$$f_w(y) = \frac{1}{y-w}\,, \quad \text{with} \quad w \in \left\{0, 1, -1, -x, -\frac{1}{x}, 1-\frac{1}{x}-x\right\}\,. \tag{A.2}$$

The weight-one HPLs are defined as

$$G(0;x) = \ln x\,, \qquad G(w;x) = \int_0^x dt f_w(t)\,. \tag{A.3}$$

HPLs of higher weight are defined by iterated integrations

$$G(w,\cdots;x) = \int_0^x dt f_w(t) G(\cdots;t)\,, \tag{A.4}$$

with the only exception being the HPLs in which all the weights are zero which are defined as follows

$$G(\underbrace{0,0,\cdots,0}_{n};x) = \frac{1}{n!}\ln^n x\,. \tag{A.5}$$

Analogous definitions hold for HPLs with argument y. The reader should be aware of the fact that in the original definition of Remiddi and Vermaseren, the weight function corresponding to the weight 1 was $f_1 = 1/(1-x)$. In order to translate the HPLs defined with the Remiddi-Vermaseren convention to the ones employed in this work (and vice versa) it is sufficient to multiply each HPL by a factor $(-1)^n$, where n is the number of weights equal to 1.

The weights $-y$ and $-1/y$ were already introduced in [28, 33, 43]. In our results, the two-dimensional harmonic polylogarithms have maximum weight four. Therefore, it was not possible to rewrite all the two-dimensional HPLs in terms of Nielsen polylogarithms, as it was done for the results of [28], where the two-dimensional HPLs had maximal weight three. However, it is possible to evaluate all the HPLs appearing in the analytic expression of the coefficient A in Eq. (2.5) by employing the `GiNaC` implementation of multiple polylogarithms by Vollinga and Weinzierl [32].

We first obtained the squared matrix elements in the non-physical region $s < 0$. The corresponding quantities in the physical region $s > 4m^2$ could be obtained by analytic

[1] The last two weights in Eq. (A.1) introduce explicit imaginary parts in the formulae. However, these HPLs appear in such a way that these imaginary parts cancel in the non-physical region, where the result has to be real. Alternatively, one could choose a basis of weight functions in which the pair $\frac{1}{2} \pm \frac{i\sqrt{3}}{2}$ is replaced by the original quadratic expressions in the integrals: $1/(x^2-x+1)$ and $x/(x^2-x+1)$ [40]. In this case these HPLs are all manifestly real.

continuation to the complex value $s \to s + i\delta$, where $\delta \to 0^+$. For $s > 4m^2$ the variable x becomes

$$x = -x' + i\delta\,, \tag{A.6}$$

where

$$x' = \frac{\sqrt{s} - \sqrt{s-4m^2}}{\sqrt{s} + \sqrt{s-4m^2}}\,, \tag{A.7}$$

So that $0 < x' < 1$ for $4m^2 < s < \infty$. The HPLs of argument x can develop an imaginary part because of analytic continuation[2]. In particular, the imaginary part of the HPLs of argument x for $s > 4m^2$ is defined when the analytic continuation of the logarithm is specified:

$$G(0;x) = G(0;-x' + i\delta) = G(0,x') + i\pi\,. \tag{A.8}$$

For notation convenience, after the analytic continuation we rename x' as x.

B. Expansion of the HPLs near the Threshold

We devote this section to a brief discussion of the technique employed to expand the coefficient A near the production threshold $\beta = \sqrt{1-4m^2/s} = 0$.

The first step consists in carrying out the analytic continuation from the non-physical region, $s < 0$, to the physical one, $s > 4m^2$, according to the method outlined above. The one- and two-dimensional HPLs appearing in the analytically continued expression of the coefficient A must then be expanded in the $\beta \to 0$ limit. While the threshold expansion of the ordinary HPLs does not lead to any particular difficulty, the expansion of the two-dimensional HPLs is indeed more delicate. The reason is that, in the latter case, the expansion parameter β appears in both the argument and the weights of the HPLs. In fact, in the physical region one finds:

$$x = \frac{1-\beta}{1+\beta}\,, \qquad y = \frac{1-\beta}{1+\beta} + \frac{4\beta}{1-\beta^2}\xi\,. \tag{B.1}$$

Moreover, the coefficient A depends on two-dimensional HPLs of maximal weight four; therefore it is very challenging to obtain explicit analytic expressions of these functions in terms of logarithms and polylogarithms of complicated arguments, which can be subsequently expanded in $\beta \to 0$. Such an approach should be replaced by a more direct and algorithmic method.

In the following we describe the method which allows to extract directly the expansion of a given two-dimensional HPL of weight n, assuming that the expansion of the HPLs of weight $n-1$ is known. Let us consider, for simplicity, the case in which the HPL has argument x and it has y (or $1/y$) in the weights. Since the dependence of x on β is the one shown in Eq. (B.1), we first use the transformation that relates $G(w,...;(1-\beta)/(1+\beta))$ to $G(w',...;\beta)$. This transformation allows to rewrite the HPL function of x as a combination

[2]The coefficient A is real for $s < 0$. However, because of the weight functions we use, and because of the fact that $0 \le y \le \infty$, individual HPLs can develop imaginary parts also in the non-physical region. The latters cancel out among each other.

of HPL functions of β, HPLs with y in the weights but evaluated in $x = 1$, and HPLs (either one- or two-dimensional) of a smaller weight. The series expansion of the HPLs with argument β is found recursively. We write them as the integral between 0 and β of the total derivative with respect to β of the HPLs themselves. The total derivative gives rise to HPLs of lower weight. We insert the expansions of the lower-weight HPLs and then we integrate again. For the HPLs evaluated in $x = 1$ the procedure is analogous. It can happen that in the intermediate steps (expansion followed by an integration) logarithmic divergences occur. These divergences must be regularized and they cancel in the final expressions.

Let us illustrate the algorithm more in detail. To this purpose, we consider the example of a simple two-dimensional HPL of weight two, which appears in the expression of the coefficient A. For $0 < x < 1$ and $x < y < 1/x$ we define

$$G(y, -1; x) = \int_0^x dt \frac{1}{t - y} G(-1, t) = \int_0^x dt \frac{1}{t - y} \ln(1 + t) \,. \tag{B.2}$$

This HPL is real in the physical region, however the intermediate stages of the procedure described below require the sum of complex terms. We assume that any ambiguity of this sort is dealt with by assigning an infinitesimal imaginary part to y. We start by rewriting the HPL of argument x in terms of HPLs of argument β; the integral representation in Eq. (B.2) can be rewritten as

$$G(y, -1; x) = G(y, -1; 1) + \int_1^x dt \frac{1}{t - y} G(-1, t) \,. \tag{B.3}$$

In the integral in the second term of Eq. (B.3) we carry out a change of integration variable by setting $q = (1 - t)/(1 + t)$ ($dt = -2/(1 + q)^2 dq$)

$$\begin{aligned} \int_1^x dt \frac{1}{t - y} G(-1, t) &= -2 \int_0^\beta dq \frac{(1 + q)}{(1 - q) - y(1 + q)} \frac{2}{(1 + q)^2} G\left(-1, \frac{1 - q}{1 + q}\right) , \\ &= \int_0^\beta dq \left(\frac{1}{q - \gamma} - \frac{1}{q + 1}\right) G\left(-1; \frac{1 - q}{1 + q}\right) , \end{aligned} \tag{B.4}$$

where we employed the relation $\beta = (1 - x)/(1 + x)$ and we introduced $\gamma = (1 - y)/(1 + y)$. We emphasize that, given the definitions of x and y in the physical region, γ is a function of β and of the variable ξ defined in Eq. (5.3). The weight one HPLs appearing in the integrand of Eq. (B.4) can also be easily rewritten in terms of HPLs of argument q:

$$G\left(-1; \frac{1 - q}{1 + q}\right) = -G(-1; q) + \ln 2 \,. \tag{B.5}$$

At this stage it is straightforward to integrate in q to finally obtain

$$\begin{aligned} G(y, -1; x) = \; & G(y, -1; 1) - \Big(G(\gamma, -1; \beta) - G(-1, -1; \beta)\Big) \\ & + \ln 2 \Big(G(\gamma; \beta) - G(-1; \beta)\Big) \,. \end{aligned} \tag{B.6}$$

In the equation above, there are one- and two-dimensional HPLs of weight one, that we consider to be known, and three HPLs of weight two. Among them, there is a single two-dimensional HPL of weight two, $G\left(\gamma(\beta), -1; \beta\right)$, and two one-dimensional HPLs. One of

them, $G(-1,-1;\beta)$, has a trivial expansion in $\beta \to 0$. Let us discuss the method employed to obtain the threshold expansion of the other two: $G\left(\gamma(\beta),-1;\beta\right)$, and $G(y,-1;1)$.

We can rewrite $G\left(\gamma(\beta),-1;\beta\right)$ as follows:

$$G\left(\gamma(\beta),-1;\beta\right) = \int_0^\beta d\beta' \frac{d}{d\beta'} G\left(\gamma(\beta'),-1;\beta'\right) + G\left(\gamma(0),-1;0\right) \,. \tag{B.7}$$

In this simple example the second term in Eq. (B.7) is well defined (and it is actually equal to zero). The derivative in the first term of Eq. (B.7) can be rewritten as

$$\begin{aligned}
\frac{d}{d\beta} G\left(\gamma(\beta),-1;\beta\right) &= \frac{1}{\beta-\gamma(\beta)} G(-1;\beta) + \int_0^\beta dt \frac{d}{d\beta}\left(\frac{1}{t-\gamma(\beta)} G(-1;t)\right) \\
&= \frac{1}{\beta-\gamma(\beta)} G(-1;\beta) + \frac{d\gamma(\beta)}{d\beta} \int_0^\beta \frac{dt}{(t-\gamma(\beta))^2} G(-1;t) \\
&= \frac{1}{\beta-\gamma(\beta)} G(-1;\beta) - \frac{d\gamma(\beta)}{d\beta} \int_0^\beta dt \frac{d}{dt}\left(\frac{1}{t-\gamma(\beta)}\right) G(-1;t) \\
&= \frac{1}{\beta-\gamma(\beta)} G(-1;\beta) - \frac{d\gamma(\beta)}{d\beta}\Bigg[\frac{1}{\beta-\gamma(\beta)} G(-1;\beta) \\
&\quad - \frac{1}{1+\gamma(\beta)} \int_0^\beta dt \left(\frac{1}{t-\gamma(\beta)} - \frac{1}{t+1}\right)\Bigg] \\
&= \frac{1}{\beta-\gamma} G(-1;\beta) - \frac{d\gamma}{d\beta}\Bigg[\frac{1}{\beta-\gamma} G(-1;\beta) - \frac{1}{1+\gamma}\Big(G(\gamma;\beta) \\
&\quad - G(-1;\beta)\Big)\Bigg] \,,
\end{aligned} \tag{B.8}$$

where in the last line we dropped the dependence of γ on β. Since the expansion of the HPLs of weight one is assumed to be known, it is straightforward to expand the equation above in the limit $\beta \to 0$ and to insert it in Eq. (B.7) to obtain

$$G\left(\gamma,-1;\beta\right) = \beta\Big[1 + (1-2\xi)\Big(\ln 2 + \ln\left(\xi\right) - \ln\left(2\xi-1\right)\Big)\Big] + \mathcal{O}(\beta^2) \,. \tag{B.9}$$

The formula above is real for $\xi > 1/2$. However, the imaginary parts which arise for $\xi < 1/2$ cancel against the imaginary parts coming from the expansion of $G(y,-1;1)$.

The expansion of $G(y,-1;1)$ can be done with the same algorithm. We write:

$$G(y(\beta),-1;1) = \int_{0^+}^\beta \frac{d}{d\beta'} G(y(\beta'),-1;1) + G(y(0^+),-1;1) \,, \tag{B.10}$$

where 0^+ indicates the fact that we must take the limit $\beta \to 0^+$ both in the integration constant and in the lower boundary of the integration. Both limits are logarithmically divergent, but the divergencies cancel between the two terms. We have:

$$\frac{d}{d\beta'} G(y(\beta'),-1;1) = \frac{dy(\beta)}{d\beta} \int_0^1 \frac{dt}{(t-y)^2} G(-1,t) \,,$$

$$= \frac{dy(\beta)}{d\beta}\left[-\frac{1}{t-y}G(-1,t)\Big|_0^1 + \frac{1}{1+y}\int_0^1 dt\left(\frac{1}{t-y}-\frac{1}{1+t}\right)\right],$$
$$= \frac{dy(\beta)}{d\beta}\left[-\frac{\ln 2}{1-y} + \frac{1}{1+y}\Big(G(y;1)-\ln 2\Big)\right]. \quad \text{(B.11)}$$

Expanding Eq. (B.11) in the limit $\beta \to 0$, we find the following Laurent series:

$$\frac{d}{d\beta'}G(y(\beta'),-1;1) = \frac{\ln 2}{\beta} + \frac{\ln 2}{2\xi-1} + (2\xi-1)\left[\ln(\beta)+\ln(2\xi-1)\right] + \mathcal{O}(\beta). \quad \text{(B.12)}$$

Integrating Eq. (B.12), as in Eq. (B.10), we find:

$$\int_{0^+}^{\beta}\frac{d}{d\beta'}G(y(\beta'),-1;1) = \ln 2\ln(\beta) - \ln 2\ln(0^+) + \beta\Bigg\{\frac{\ln 2}{2\xi-1} + (2\xi-1)\Big[\ln(\beta) + \ln(2\xi-1) - 1\Big]\Bigg\} + \mathcal{O}(\beta^2). \quad \text{(B.13)}$$

Moreover, one finds:

$$G(y(0^+),-1;1) = G(y(0^+);1)G(-1;1) - G(-1,y(0^+);1),$$
$$= \ln 2\left[\ln(0^+)+\ln 2+\ln(2\xi-1)\right] + \frac{1}{2}\zeta_2 - \frac{1}{2}\ln^2 2. \quad \text{(B.14)}$$

Finally, we have:

$$G(y(\beta),-1;1) = \ln 2\ln(\beta) + \ln 2\ln(2\xi-1) + \frac{1}{2}\ln^2 2 + \frac{1}{2}\zeta_2 + \beta\Bigg\{\frac{\ln 2}{2\xi-1} + (2\xi-1)\Big[\ln(\beta)+\ln(2\xi-1)-1\Big]\Bigg\} + \mathcal{O}(\beta^2), \quad \text{(B.15)}$$

where the divergencies disappeared. Considering also the expansion of the one- and two-dimensional HPLs of weight 1 and the expansion of $G(-1,-1;\beta)$ in Eq. (B.6), we find the final formula:

$$G(y,-1;x) = \ln 2\ln(\beta) + \ln 2\ln(\xi) + \frac{3}{2}\ln^2 2 + \frac{1}{2}\zeta_2 + \beta\Big\{-2\xi + (2\xi-1)[\ln(\beta)+\ln(\xi)+\ln 2]\Big\} + \mathcal{O}(\beta^2). \quad \text{(B.16)}$$

In the case in which the argument of the HPLs is y and x is present in the weights, $G(w,...;y)$, the procedure is analogous to the one explained above. Since the dependence of y on β involves also the parameter ξ (see Eq. (B.1)), the first step consists in using the scale properties of the HPLs:

$$G(w,...;y) = G(\lambda w,...;\lambda y), \quad \text{(B.17)}$$

(valid in the case in which all the trailing zeroes have already been extracted) to get rid of the ξ dependence in the argument. To achieve this goal, one multiplies weights and argument by

$$\lambda = \frac{1}{1+\frac{4\beta}{(1-\beta)^2}\xi}. \quad \text{(B.18)}$$

In so doing, we fit again in the case illustrated in the example concerning $G(w,...;x)$, since

$$\frac{1}{1+\frac{4\beta}{(1-\beta)^2}\xi}\,y=\frac{1-\beta}{1+\beta}\,, \tag{B.19}$$

and the expansion proceeds along the same steps as outlined above.

C. Master Integrals

In this Appendix we collect the MIs for the topologies in Fig. 3.

The explicit expression of the MIs depends on the chosen normalization of the integration measure. The integration on the loop momenta is normalized as follows:

$$\int \mathfrak{D}^d k = \frac{1}{C(\varepsilon)}\left(\frac{\mu^2}{m^2}\right)^{-\varepsilon}\mu^{2\varepsilon}\int\frac{d^dk}{(4\pi^2)^{(1-\varepsilon)}}\,, \tag{C.1}$$

where $C(\varepsilon)$ was defined in Eq. (5.1). In Eq. (C.1) μ stands for the 't Hooft mass of dimensional regularization. The integration measure in Eq. (C.1) is chosen in such a way that the one-loop massive tadpole becomes

$$\int \mathfrak{D}^d k\;\frac{1}{k^2+m^2}=-\frac{m^2}{4(1-\varepsilon)\varepsilon}\,. \tag{C.2}$$

In calculating the squared matrix element, we multiply our bare results by $(\mu^2/m^2)^\varepsilon$, in order to make explicit the dependence on the 't Hooft scale. We also point out that, since the squared matrix element still contains soft and collinear divergencies regulated by ε, it depends on the normalization of the integration measure. In particular, in order to match our results with the ones of [25, 27], it is necessary to multiply the latter by the factor

$$\frac{e^{-2\gamma\varepsilon}}{\Gamma\left(1+\varepsilon\right)^2}=1-\zeta(2)\varepsilon^2+\frac{2}{3}\zeta(3)\varepsilon^3+\frac{3}{10}\zeta(2)^2\varepsilon^4+\mathcal{O}\left(\varepsilon^5\right)\,. \tag{C.3}$$

The MIs are expanded in powers of the dimensional regulator ε; below we collect the analytic expression of the coefficients in the ε expansion up to terms involving HPLs and 2dHPLs of weight three. The coefficients involving HPLs and 2dHPLs of weight four are also needed in order to obtain the finite part of the leading color coefficient, and we calculated them. However, their analytic expressions are too long to be written in this appendix; the interested reader can find them in the text file included in the arXiv submission of this paper.

There are two MIs belonging to the topology Fig. 3-(a). The first MI is

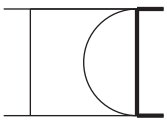

$$= \int \frac{\mathfrak{D}^d k_1 \mathfrak{D}^d k_2}{P_0\left(k_2\right) P_0\left(k_1-k_2\right) P_0\left(k_2-p_1\right) P_0\left(k_2-p_1-p_2\right) P_m\left(k_1-p_3\right)}\,, \tag{C.4}$$

where we define

$$P_0\left(k\right)\equiv k^2\,,\qquad P_m\left(k\right)\equiv k^2+m^2\,. \tag{C.5}$$

We find

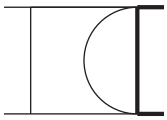

$$= \frac{1}{m^2}\sum_{i=-3}^{0} A_i \varepsilon^i + \mathcal{O}(\varepsilon)\,, \tag{C.6}$$

$$\begin{aligned}
A_{-3} &= \frac{x}{16(1-x)^2}\,,\\
A_{-2} &= -\frac{x}{16(1-x)^2 y}\Big[-2y - yG(0;x) + 2yG(1;x) + (y+1)G(-1;y)\Big]\,,\\
A_{-1} &= -\frac{x}{16(1-x)^2 y}\Big[y(3\zeta(2)-4) + 2(y+1)G(-1;y) - 2yG(0;x)\\
&\quad +(y+1)coeffA.texG(-1;y)G(0;x) + 4yG(1;x) - 2(y+1)G(-1;y)G(1;x)\\
&\quad -2(y+1)G(-1,-1;y) + (y-1)G(0,-1;y) - yG(0,0;x) + 2yG(0,1;x)\\
&\quad +2yG(1,0;x) - 4yG(1,1;x)\Big]\,,\\
A_0 &= -\frac{x}{16(1-x)^2 y}\Big[2y(3\zeta(2)+7\zeta(3)-4) - (7\zeta(2)y - 4y + 11\zeta(2) - 4)G(-1;y)\\
&\quad -y(\zeta(2)+4)G(0;x) + 2(y+1)G(-1;y)G(0;x) - 2y(3\zeta(2)-4)G(1;x)\\
&\quad -4(y+1)G(-1;y)G(1;x) + 4(y+1)\zeta(2)G\left(-1/y;x\right) - 4(y+1)G(-1,-1;y)\\
&\quad -4(y+1)G(0;x)G(-1,-1;y) + 4(y+1)G(1;x)G(-1,-1;y)\\
&\quad +2(y+1)G\left(-1/y;x\right)G(-1,-1;y) + 2(y+1)G(-y;x)G(-1,-1;y)\\
&\quad +2(y-1)G(0,-1;y) + 2yG(0;x)G(0,-1;y) - 2(y-1)G(1;x)G(0,-1;y)\\
&\quad -(y+1)G\left(-1/y;x\right)G(0,-1;y) - (y+1)G(-y;x)G(0,-1;y) - 2yG(0,0;x)\\
&\quad +4yG(0,1;x) + 4yG(1,0;x) - 2(y+1)G(-1;y)G(1,0;x) - 8yG(1,1;x)\\
&\quad +4(y+1)G(-1;y)G(1,1;x) + (y+1)G(-1;y)G\left(-1/y,0;x\right)\\
&\quad -2(y+1)G(-1;y)G\left(-1/y,1;x\right) + (y+1)G(-1;y)G(-y,0;x)\\
&\quad -2(y+1)G(-1;y)G(-y,1;x) + 2(y-1)G(-1,0,-1;y) + 4G(0,-1,-1;y)\\
&\quad -2yG(0,0,-1;y) - 2yG(0,0,0;x) + 4yG(0,0,1;x) + (3y+1)G(0,1,0;x)\\
&\quad -2(3y+1)G(0,1,1;x) + 2yG(1,0,0;x) - 4yG(1,0,1;x) - 4yG(1,1,0;x)\\
&\quad +8yG(1,1,1;x) + (y+1)G\left(-1/y,0,0,x\right) - 2(y+1)G\left(-1/y,0,1;x\right)\\
&\quad -(y+1)G\left(-1/y,1,0;x\right) + 2(y+1)G\left(-1/y,1,1,x\right) - (y+1)G(-y,1,0;x)\\
&\quad +2(y+1)G(-y,1,1;x)\Big]\,.
\end{aligned} \tag{C.7}$$

The second MI for the topology in Fig. 3-(a) was chosen as

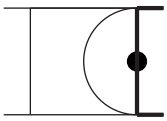

$$= \int \frac{\mathfrak{D}^d k_1 \mathfrak{D}^d k_2}{P_0\left(k_2\right) P_0\left(k_1-k_2\right) P_0\left(k_2-p_1\right) P_0\left(k_2-p_1-p_2\right) P_m^2\left(k_1-p_3\right)}\,. \tag{C.8}$$

Its analytic expression is

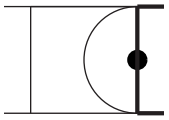

$$= \frac{1}{m^4}\sum_{i=-2}^{0} A_i\varepsilon^i + \mathcal{O}(\varepsilon)\,, \tag{C.9}$$

$$\begin{aligned}
A_{-2} &= \frac{x}{16(1-x)^2 y}G(-1;y)\,,\\
A_{-1} &= -\frac{x}{16(1-x)^2 y}\Big[-G(-1;y)G(0;x)+2G(-1;y)G(1;x)+2G(-1,-1;y)\\
&\quad +G(0,-1;y)\Big]\,,\\
A_0 &= -\frac{x}{16(1-x)^2 y}\Big[11\zeta(2)G(-1;y)+2G(1,0;x)G(-1;y)-4G(1,1;x)G(-1;y)\\
&\quad -G\left(-1/y,0;x\right)G(-1;y)+2G\left(-1/y,1;x\right)G(-1;y)-G(-y,0;x)G(-1;y)\\
&\quad +2G(-y,1;x)G(-1;y)-4\zeta(2)\;G\left(-1/y;x\right)+4G(0;x)G(-1,-1;y)\\
&\quad -4G(1;x)G(-1,-1;y)-2G\left(-1/y;x\right)G(-1,-1;y)-2G(-y;x)G(-1,-1;y)\\
&\quad -2G(1;x)G(0,-1;y)+G\left(-1/y;x\right)G(0,-1;y)+G(-y;x)G(0,-1;y)\\
&\quad +2G(-1,0,-1;y)-4G(0,-1,-1;y)-G(0,1,0;x)+2G(0,1,1;x)\\
&\quad -G\left(-1/y,0,0;x\right)+2G\left(-1/y,0,1;x\right)+G\left(-1/y,1,0;x\right)\\
&\quad -2G\left(-1/y,1,1;x\right)+G(-y,1,0;x)-2G(-y,1,1;x)\Big]\,.
\end{aligned} \tag{C.10}$$

The topology shown in Fig. 3-(b) has two MIs. The first one,

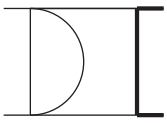

$$= \int \frac{\mathfrak{D}^d k_1 \mathfrak{D}^d k_2}{P_0\left(k_1\right) P_0\left(k_1-k_2\right) P_0\left(k_2-p_1\right) P_0\left(k_1-p_1-p_2\right) P_m\left(k_1-p_3\right)}\,, \tag{C.11}$$

has the following analytic expression:

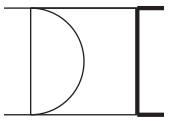

$$= \frac{1}{m^2}\sum_{i=-1}^{0} A_i\varepsilon^i + \mathcal{O}(\varepsilon)\,, \tag{C.12}$$

$$\begin{aligned}
A_{-1} &= \frac{x}{16(1-x^2)}\left[4\zeta(2)+G(0,0;x)-2G(0,1;x)\right]\,,\\
A_0 &= \frac{x}{16(1-x^2)}\Big[\zeta(2)\Big(16G(-1;x)-G(0;x)-12G(1;x)-4\;G\left(-1/y;x\right)+8\Big)\\
&\quad +7\zeta(3)-2\;G\left(-1/y;x\right)G(-1,-1;y)+2G(-y;x)G(-1,-1;y)\\
&\quad +G(0;x)G(0,-1;y)+G\left(-1/y;x\right)G(0,-1;y)-G(-y;x)G(0,-1;y)+2\;G(0,0;x)\\
&\quad -4G(0,1;x)-G(-1;y)G\left(-1/y,0;x\right)+2G(-1;y)\;G\left(-1/y,1;x\right)\\
&\quad +G(-1;y)G(-y,0;x)-2G(-1;y)\;G(-y,1;x)+4G(-1,0,0;x)-8G(-1,0,1;x)\\
&\quad +2G(0,-1,-1;y)-G(0,0,-1;y)+2\;G(0,0,0;x)-4G(0,0,1;x)-4G(0,1,0;x)
\end{aligned}$$

$$
\begin{aligned}
&+8G(0,1,1;x) - 3G(1,0,0;x) + 6\ G(1,0,1;x) - G\left(-1/y,0,0;x\right)\\
&+2G\left(-1/y,0,1;x\right) + G\left(-1/y,1,0;x\right) - 2G\ \ \left(-1/y,1,1;x\right) - G(-y,1,0;x)\\
&+2G(-y,1,1;x)\Big]\,. \qquad \text{(C.13)}
\end{aligned}
$$

The second MI for the topology in Fig. 3-(b) is:

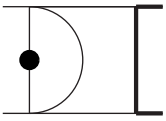

$$
= \int \frac{\mathfrak{D}^d k_1 \mathfrak{D}^d k_2}{P_0\left(k_1\right) P_0^2\left(k_1-k_2\right) P_0\left(k_2-p_1\right) P_0\left(k_1-p_1-p_2\right) P_m\left(k_1-p_3\right)}\,, \qquad \text{(C.14)}
$$

where

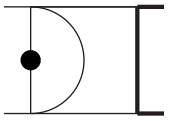

$$
= \frac{1}{m^4}\sum_{i=-3}^{0} A_i \varepsilon^i + \mathcal{O}(\varepsilon)\,, \qquad \text{(C.15)}
$$

$$
\begin{aligned}
A_{-3} &= -\frac{7x}{192(1-x)^2(1+y)}\,,\\
A_{-2} &= -\frac{x}{96(1-x)^2(1+y)}\Big[-8G(-1;y) + 3G(0;x) - 6G(1;x)\Big]\,,\\
A_{-1} &= -\frac{x}{24(1-x)^2(1+y)}\Big[-5\zeta(2) - 3G(-1;y)G(0;x) + 6G(-1;y)G(1;x)\\
&\quad +2G(-1,-1;y)\Big]\,,\\
A_{0} &= -\frac{x}{48(1-x)^2(1+y)}\Big[-29\zeta(3) + 46\zeta(2)G(-1;y) + 3\zeta(2)G(0;x)\\
&\quad +30\zeta(2)G(1;x) - 36\zeta(2)G\left(-1/y;x\right) + 24G(0;x)G(-1,-1;y)\\
&\quad -12G(1;x)G(-1,-1;y) - 18G\left(-1/y;x\right)G(-1,-1;y) - 18G(-y;x)G(-1,-1;y)\\
&\quad -9G(0;x)G(0,-1;y) + 9G\left(-1/y;x\right)G(0,-1;y) + 9G(-y;x)G(0,-1;y)\\
&\quad +18G(-1;y)G(1,0;x) - 36G(-1;y)G(1,1;x) - 9G(-1;y)G\left(-1/y,0;x\right)\\
&\quad +18G(-1;y)G\left(-1/y,1;x\right) - 9G(-1;y)G(-y,0;x) + 18G(-1;y)G(-y,1;x)\\
&\quad +32G(-1,-1,-1;y) - 18G(-1,0,-1;y) - 18G(0,-1,-1;y) + 9G(0,0,-1;y)\\
&\quad +9G(1,0,0;x) - 18G(1,0,1;x) - 18G(1,1,0;x) + 36G(1,1,1;x)\\
&\quad -9G\left(-1/y,0,0;x\right) + 18G\left(-1/y,0,1;x\right) + 9G\left(-1/y,1,0;x\right)\\
&\quad -18G\left(-1/y,1,1;x\right) + 9G(-y,1,0;x) - 18G(-y,1,1;x)\Big]\,. \qquad \text{(C.16)}
\end{aligned}
$$

The are two MIs for the topology in Fig. 3-(c). The first one is

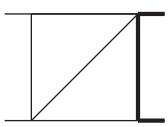

$$
= \int \frac{\mathfrak{D}^d k_1 \mathfrak{D}^d k_2}{P_0\left(k_2\right) P_0\left(k_1-k_2\right) P_0\left(k_2-p_1\right) P_0\left(k_1-p_1-p_2\right) P_m\left(k_1-p_3\right)}\,, \qquad \text{(C.17)}
$$

and the corresponding Laurent expansion in ε is

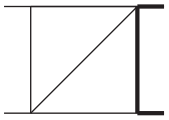

$$= \frac{1}{m^2}\frac{A_{-1}}{\varepsilon} + \mathcal{O}(\varepsilon^0)\,, \tag{C.18}$$

$$\begin{aligned}
A_{-1} = -\frac{x}{16(1-x+x^2+xy)}\Big[&\zeta(3) + \zeta(2)G(-1;y) - 3\zeta(2)G(0;x)\\
&-6\zeta(2)G(1;x) + 4\zeta(2)G\left(-1/y;x\right) - 4G(1;x)G(-1,-1;y)\\
&+2G\left(-1/y;x\right)G(-1,-1;y) + 2G(-y;x)G(-1,-1;y) + G(0;x)G(0,-1;y)\\
&-G\left(-1/y;x\right)G(0,-1;y) - G(-y;x)G(0,-1;y) - 2G(-1;y)G(1,0;x)\\
&+4G(-1;y)G(1,1;x) + G(-1;y)G\left(-1/y,0;x\right) - 2G(-1;y)G\left(-1/y,1;x\right)\\
&+G(-1;y)G(-y,0;x) - 2G(-1;y)G(-y,1;x) + G(-1,0,-1;y)\\
&+2G(0,-1,-1;y) - G(0,0,-1;y) - G(0,0,0;x) + 2G(0,0,1;x)\\
&-G(1,0,0;x) + 2G(1,0,1;x) + 2G(1,1,0;x) - 4G(1,1,1;x)\\
&+G\left(-1/y,0,0;x\right) - 2G\left(-1/y,0,1;x\right) - G\left(-1/y,1,0;x\right)\\
&+2G\left(-1/y,1,1;x\right) - G(-y,1,0;x) + 2G(-y,1,1;x)\Big]\,.
\end{aligned} \tag{C.19}$$

The second MI for the topology in Fig. 3-(c) was chosen to be

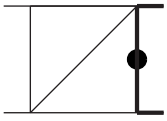

$$= \int \frac{\mathfrak{D}^d k_1 \mathfrak{D}^d k_2}{P_0\left(k_2\right) P_0\left(k_1-k_2\right) P_0\left(k_2-p_1\right) P_0\left(k_1-p_1-p_2\right) P_m^2\left(k_1-p_3\right)}\,, \tag{C.20}$$

where

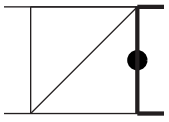

$$= \frac{1}{m^4}\sum_{i=-3}^{0} A_i \varepsilon^i + \mathcal{O}(\varepsilon)\,, \tag{C.21}$$

$$\begin{aligned}
A_{-3} &= -\frac{x}{96(1-x)^2}\,,\\
A_{-2} &= \frac{x}{96(1-x)^2}\Big[-2G(-1;y) - 3G(0;x) + 6G(1;x)\Big]\,,\\
A_{-1} &= \frac{x}{96(1-x)^2}\Big[-11\zeta(2) - 6G(-1;y)G(0;x) + 12G(-1;y)G(1;x) - 4G(-1,-1;y)\\
&\quad -9G(0,0;x) + 18G(0,1;x) + 18G(1,0;x) - 36G(1,1;x)\Big]\,,\\
A_{-0} &= \frac{x}{96(1-x)^2}\Big[-34\zeta(3) + 50\zeta(2)G(-1;y) + 39\zeta(2)G(0;x) + 66\zeta(2)G(1;x)\\
&\quad -72\zeta(2)G\left(-1/y;x\right) + 24G(0;x)G(-1,-1;y) + 24G(1;x)G(-1,-1;y)\\
&\quad -36G\left(-1/y;x\right)G(-1,-1;y) - 36G(-y;x)G(-1,-1;y) - 18G(0;x)G(0,-1;y)\\
&\quad +18G\left(-1/y;x\right)G(0,-1;y) + 18G(-y;x)G(0,-1;y) + 36G(-1;y)G(1,0;x)
\end{aligned}$$

$$
\begin{aligned}
&-72G(-1;y)G(1,1;x) - 18G(-1;y)G\left(-1/y,0;x\right) + 36G(-1;y)G\left(-1/y,1;x\right)\\
&-18G(-1;y)G(-y,0;x) + 36G(-1;y)G(-y,1;x) + 64G(-1,-1,-1;y)\\
&-36G(-1,0,-1;y) - 36G(0,-1,-1;y) + 18G(0,0,-1;y) - 9G(0,0,0;x)\\
&+18G(0,0,1;x) + 36G(0,1,0;x) - 72G(0,1,1;x) + 54G(1,0,0;x)\\
&-108G(1,0,1;x) - 108G(1,1,0;x) + 216G(1,1,1;x) - 18G\left(-1/y,0,0;x\right)\\
&+36G\left(-1/y,0,1;x\right) + 18G\left(-1/y,1,0;x\right) - 36G\left(-1/y,1,1;x\right)\\
&+18G(-y,1,0;x) - 36G(-y,1,1;x)\Big] \,. \qquad \text{(C.22)}
\end{aligned}
$$

The topology shown in Fig. 3-(d) has two MIs. The first one is

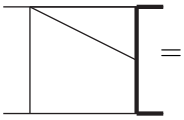

$$
= \int \frac{\mathfrak{D}^d k_1 \mathfrak{D}^d k_2}{P_0(k_2)\, P_0(k_1-k_2)\, P_0(k_1-p_1)\, P_0(k_1-p_1-p_2)\, P_m(k_1-p_3)\, P_m(k_2-p_3)} \,, \qquad \text{(C.23)}
$$

with

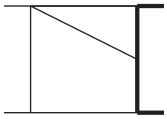

$$
= \frac{1}{m^4} \sum_{i=-2}^{-1} A_i \varepsilon^i + \mathcal{O}(\varepsilon^0) \,, \qquad \text{(C.24)}
$$

$$
\begin{aligned}
A_{-2} =& -\frac{x}{32(1-x^2)(1+y)}\Big[-4\zeta(2) - G(0,0;x) + 2G(0,1;x)\Big] \,,\\
A_{-1} =& -\frac{x}{32(1-x^2)(1+y)}\Big[-5\zeta(3) + 8\zeta(2)G(-1;x) + 8\zeta(2)G(-1;y) - 3\zeta(2)G(0;x)\\
&+16\zeta(2)G(1;x) - 8\zeta(2)\; G\left(-1/y;x\right) - 4G\left(-1/y;x\right)\; G(-1,-1;y)\\
&+4G(-y;x)G(-1,-1;y) + 2G(0;x)G(0,-1;y) + 2G\left(-1/y;x\right)G(0,-1;y)\\
&-2G(-y;x)G(0,-1;y) + 2G(-1;y)G(0,0;x) - 4G(-1;y)G(0,1;x)\\
&-2G(-1;y)\; G\left(-1/y,0;x\right) + 4G(-1;y)G\left(-1/y,1;x\right) + 2G(-1;y)G(-y,0;x)\\
&-4G(-1;y)G(-y,1;x) + 2G(-1,0,0;x) - 4G(-1,0,1;x) + 4G(0,-1,-1;y)\\
&-2G(0,0,-1;y) - 3G(0,0,0;x) + 6G(0,0,1;x) + 2G(0,1,0;x)\\
&-4G(0,1,1;x) + 4G(1,0,0;x) - 8G(1,0,1;x) - 2G\left(-1/y,0,0;x\right)\\
&+4G\left(-1/y,0,1;x\right) + 2G\left(-1/y,1,0;x\right) - 4G\left(-1/y,1,1;x\right) - 2G(-y,1,0;x)\\
&+4G(-y,1,1;x)\Big] \,. \qquad \text{(C.25)}
\end{aligned}
$$

The second MI for topology 3-(d) is

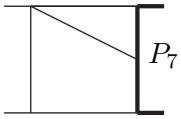

$$
P_7 = \int \frac{\mathfrak{D}^d k_1 \mathfrak{D}^d k_2 (k_2-p_1-p_2)^2}{P_0(k_2)\, P_0(k_1-k_2)\, P_0(k_1-p_1)\, P_0(k_1-p_1-p_2)\, P_m(k_1-p_3)\, P_m(k_2-p_3)} \,, \qquad \text{(C.26)}
$$

where

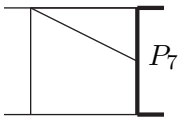

$$= \frac{1}{m^2}\sum_{i=-3}^{0} A_i \varepsilon^i + \mathcal{O}(\varepsilon)\,, \tag{C.27}$$

$$\begin{aligned}
A_{-3} &= \frac{1}{32(1+y)}\,,\\
A_{-2} &= \frac{1}{16(1+y)}\Big[1 - G(-1;y)\Big]\,,\\
A_{-1} &= \frac{1}{16(1+y)(x+1)}\Big[5\zeta(2)x + 2x - 3\zeta(2) + 2 - 2(x+1)G(-1;y)\\
&\quad +2(x+1)G(-1,-1;y) + (x-1)G(0,0;x) - 2(x-1)G(0,1;x)\Big]\,,\\
A_0 &= \frac{1}{16(1+y)(x+1)(1-x+x^2+xy)}\Big[8(x+1)(x-1)^2G(1;x)G(-1,-1;y)\\
&\quad +4(x+1)(x-1)^2G(-1;y)G(1,0;x) - 8(x+1)(x-1)^2G(-1;y)G(1,1;x)\\
&\quad -4(x+1)(x-1)^2G(1,1,0;x) + 8(x+1)(x-1)^2G(1,1,1;x)\\
&\quad -8\left(x^2+yx-x+1\right)(x-1)\zeta(2)G(-1;x) + 3\left(3x^2+yx-x-1\right)(x-1)\zeta(2)G(0;x)\\
&\quad -4\left(x^2+4yx-4x+7\right)(x-1)\zeta(2)G(1;x) + 8(yx-x+2)(x-1)\zeta(2)G\left(-1/y;x\right)\\
&\quad +4(yx-x+2)(x-1)G\left(-1/y;x\right)G(-1,-1;y) - 4x(2x+y-1)\times\\
&\quad \times(x-1)G(-y;x)G(-1,-1;y) - 2x(2x+y-1)(x-1)G(0;x)G(0,-1;y)\\
&\quad -2(yx-x+2)(x-1)G\left(-1/y;x\right)G(0,-1;y) + 2x(2x+y-1)(x-1)\times\\
&\quad \times G(-y;x)G(0,-1;y) + 2\left(x^2+yx-x+1\right)(x-1)G(0,0;x) - 2\left(x^2+yx-x+1\right)\times\\
&\quad \times(x-1)G(-1;y)G(0,0;x) - 4\left(x^2+yx-x+1\right)(x-1)G(0,1;x)\\
&\quad +4\left(x^2+yx-x+1\right)(x-1)G(-1;y)G(0,1;x) + 2(yx-x+2)(x-1)G(-1;y)\\
&\quad G\left(-1/y,0;x\right) - 4(yx-x+2)(x-1)G(-1;y)G\left(-1/y,1;x\right)\\
&\quad -2x(2x+y-1)(x-1)G(-1;y)G(-y,0;x) + 4x(2x+y-1)(x-1)G(-1;y)\times\\
&\quad \times G(-y,1;x) - 2\left(x^2+yx-x+1\right)(x-1)G(-1,0,0;x) + 4\left(x^2+yx-x+1\right)\times\\
&\quad \times(x-1)G(-1,0,1;x) + 2x(2x+y-1)(x-1)G(0,0,-1;y) + (5x^2+3yx\\
&\quad -3x+1)(x-1)G(0,0,0;x) - 2\left(5x^2+3yx-3x+1\right)(x-1)G(0,0,1;x)\\
&\quad -2\left(x^2+yx-x+1\right)(x-1)G(0,1,0;x) + 4\left(x^2+yx-x+1\right)(x-1)G(0,1,1;x)\\
&\quad -2\left(x^2+2yx-2x+3\right)(x-1)G(1,0,0;x) + 4(x^2+2yx-2x\\
&\quad +3)(x-1)G(1,0,1;x) + 2(yx-x+2)G\left(-1/y,0,0;x\right)(x-1) - 4(yx-x\\
&\quad +2)(x-1)G\left(-1/y,0,1;x\right) - 2(yx-x+2)(x-1)G\left(-1/y,1,0;x\right) + 4(yx-x\\
&\quad +2)(x-1)G\left(-1/y,1,1;x\right) + 2x(2x+y-1)(x-1)G(-y,1,0;x) - 4x(2x+y\\
&\quad -1)(x-1)G(-y,1,1;x) + 2(5\zeta(2)x^3 + 4\zeta(3)x^3 + 2x^3 + 2yx^2 + 5y\zeta(2)x^2\\
&\quad -8\zeta(2)x^2 + 5y\zeta(3)x^2 - 4\zeta(3)x^2 + 2yx - 3y\zeta(2)x + 8\zeta(2)x + 6\zeta(3)x - 3\zeta(2) - \zeta(3)
\end{aligned}$$

$$
\begin{aligned}
&+2) - 2(5\zeta(2)x^3 + 2x^3 + 2yx^2 + 4y\zeta(2)x^2 - 9\zeta(2)x^2 + 2yx - 4y\zeta(2)x + 7\zeta(2)x \\
&-3\zeta(2) + 2)G(-1;y) + 4(x+1)\left(x^2 + yx - x + 1\right)G(-1,-1;y) - 4(x+1)(x^2 \\
&+yx - x + 1)G(-1,-1,-1;y) + 2x(x+1)(y+1)G(-1,0,-1;y) - 2(5x^3 + 3yx^2 \\
&-6x^2 - yx + 2x + 1)G(0,-1,-1;y)\Big] \,. \qquad \text{(C.28)}
\end{aligned}
$$

The topology in Fig. 3-(e) involves two MIs. One of them is

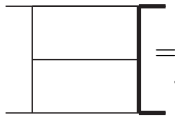

$$
= \int \frac{\mathfrak{D}^d k_1 \mathfrak{D}^d k_2}{P_0(k_2) P_0(k_1 - k_2) P_0(k_1 - p_1) P_0(k_2 - p_1) P_0(k_1 - p_1 - p_2) P_m(k_1 - p_3) P_m(k_2 - p_3)} \,, \qquad \text{(C.29)}
$$

where

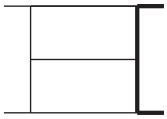

$$
= \frac{1}{m^6} \sum_{i=-4}^{-1} A_i \varepsilon^i + \mathcal{O}(\varepsilon^0) \,, \qquad \text{(C.30)}
$$

$$
\begin{aligned}
A_{-4} &= \frac{x}{12(1-x)^2(1+y)^2} \,, \\
A_{-3} &= \frac{x}{96(1-x)^2(1+y)^2}\Big[-14G(-1;y) + 9G(0;x) - 18G(1;x)\Big] \,, \\
A_{-2} &= \frac{x}{48(1-x)^2(1+y)^2}\Big[-22\zeta(2) - 12G(-1;y)G(0;x) + 24G(-1;y)G(1;x) \\
&\quad +4G(-1,-1;y) + 3G(0,0;x) - 6G(0,1;x) - 6G(1,0;x) + 12G(1,1;x)\Big] \,, \\
A_{-1} &= \frac{x}{48(1-x)^2(1+y)^2}\Big[-29\zeta(3) + 46\zeta(2)G(-1;y) - 21\zeta(2)G(0;x) \\
&\quad +66\zeta(2)G(1;x) - 24\zeta(2)G\left(-1/y;x\right) + 24G(0;x)G(-1,-1;y) \\
&\quad -24G(1;x)G(-1,-1;y) - 12G\left(-1/y;x\right)G(-1,-1;y) \\
&\quad -12G(-y;x)G(-1,-1;y) - 6G(0;x)G(0,-1;y) + 6G\left(-1/y;x\right)G(0,-1;y) \\
&\quad +6G(-y;x)G(0,-1;y) - 12G(-1;y)G(0,0;x) + 24G(-1;y)G(0,1;x) \\
&\quad +36G(-1;y)G(1,0;x) - 72G(-1;y)G(1,1;x) - 6G(-1;y)G\left(-1/y,0;x\right) \\
&\quad +12G(-1;y)G\left(-1/y,1;x\right) - 6G(-1;y)G(-y,0;x) + 12G(-1;y)G(-y,1;x) \\
&\quad +32G(-1,-1,-1;y) - 12G(-1,0,-1;y) - 12G(0,-1,-1;y) \\
&\quad +6G(0,0,-1;y) + 6G(1,0,0;x) - 12G(1,0,1;x) - 12G(1,1,0;x) \\
&\quad +24G(1,1,1;x) - 6G\left(-1/y,0,0;x\right) + 12G\left(-1/y,0,1;x\right) + 6G\left(-1/y,1,0;x\right) \\
&\quad -12G\left(-1/y,1,1;x\right) + 6G(-y,1,0;x) - 12G(-y,1,1;x)\Big] \,. \qquad \text{(C.31)}
\end{aligned}
$$

The second MI for the topology in Fig. 3-(e) is

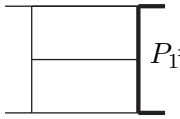

$$
= \int \frac{\mathfrak{D}^d k_1 \mathfrak{D}^d k_2 \, k_1^2}{P_0(k_2) P_0(k_1 - k_2) P_0(k_1 - p_1) P_0(k_2 - p_1) P_0(k_1 - p_1 - p_2) P_m(k_1 - p_3) P_m(k_2 - p_3)} \,, \qquad \text{(C.32)}
$$

where

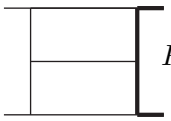

$$= \frac{1}{m^4}\sum_{i=-4}^{-1} A_i\varepsilon^i + \mathcal{O}(\varepsilon^0)\,, \tag{C.33}$$

$$\begin{aligned}
A_{-4} &= \frac{1}{24(1+y)^2}\,,\\
A_{-3} &= \frac{1}{96(1+y)^2}\Big[-10G(-1;y)+3G(0;x)-6G(1;x)\Big]\,,\\
A_{-2} &= \frac{1}{192(1+y)^2}\Big[-47\zeta(2)-24G(-1;y)G(0;x)+48G(-1;y)G(1;x)+32G(-1,-1;y)\\
&\quad -6G(0,-1;y)\Big]\,,\\
A_{-1} &= \frac{1}{192(1+y)^2}\Big[-85\zeta(3)+188\zeta(2)G(-1;y)+96\zeta(2)G(1;x)-96\zeta(2)\;G\left(-1/y;x\right)\\
&\quad +96G(0;x)G(-1,-1;y)-96G(1;x)G(-1,-1;y)-48G\left(-1/y;x\right)G(-1,-1;y)\\
&\quad -48G(-y;x)G(-1,-1;y)-24G(0;x)G(0,-1;y)+24G\left(-1/y;x\right)G(0,-1;y)\\
&\quad +24G(-y;x)G(0,-1;y)+48G(-1;y)G(1,0;x)-96G(-1;y)G(1,1;x)\\
&\quad -24G(-1;y)G\left(-1/y,0;x\right)+48G(-1;y)G\left(-1/y,1;x\right)-24G(-1;y)G(-y,0;x)\\
&\quad +48G(-1;y)G(-y,1;x)+64G(-1,-1,-1;y)-24G(-1,0,-1;y)\\
&\quad -12G(0,-1,-1;y)+6G(0,0,-1;y)+24G(1,0,0;x)-48G(1,0,1;x)\\
&\quad -48G(1,1,0;x)+96G(1,1,1;x)-24G\left(-1/y,0,0;x\right)+48G\left(-1/y,0,1;x\right)\\
&\quad +24G\left(-1/y,1,0;x\right)-48G\left(-1/y,1,1;x\right)+24G(-y,1,0;x)-48G(-y,1,1;x)\Big]\,.
\end{aligned} \tag{C.34}$$

Finally, the topology in Fig. 3-(f) involves three MIs. The first MI we chose is

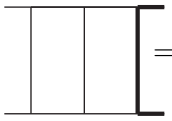

$$= \int \frac{\mathfrak{D}^d k_1 \mathfrak{D}^d k_2}{P_0(k_1)P_0(k_2)P_0(k_1-k_2)P_0(k_2-p_1)P_0(k_1-p_1-p_2)P_0(k_2-p_1-p_2)P_m(k_1-p_3)}\,, \tag{C.35}$$

where

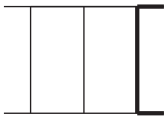

$$= \frac{1}{m^6}\sum_{i=-4}^{-1} A_i\varepsilon^i + \mathcal{O}(\varepsilon^0)\,, \tag{C.36}$$

$$\begin{aligned}
A_{-4} &= \frac{x^2}{24(1-x)^4(1+y)}\,,\\
A_{-3} &= \frac{x^2}{96(1-x)^4(1+y)}\Big[-10G(-1;y)+3G(0;x)-6G(1;x)\Big]\,,
\end{aligned}$$

$$
\begin{aligned}
A_{-2} =& \frac{x^2}{48(1-x)^4(1+y)}\Big[-5\zeta(2) - 6G(-1;y)G(0;x)+12G(-1;y)G(1;x)+8G(-1,-1;y)\Big]\,,\\
A_{-1} =& \frac{x^2}{48(1-x)^4(1+y)}\Big[-13\zeta(3) + 38\zeta(2)G(-1;y) + 9\zeta(2)G(0;x) + 6\zeta(2)G(1;x)\\
&-24\zeta(2)G\left(-1/y;x\right) + 24G(0;x)G(-1,-1;y) - 24G(1;x)G(-1,-1;y)\\
&-12G\left(-1/y;x\right)G(-1,-1;y) - 12G(-y;x)G(-1,-1;y) - 6G(0;x)G(0,-1;y)\\
&+6G\left(-1/y;x\right)G(0,-1;y) + 6G(-y;x)G(0,-1;y) + 12G(-1;y)G(1,0;x)\\
&-24G(-1;y)G(1,1;x) - 6G(-1;y)G\left(-1/y,0;x\right) + 12G(-1;y)G\left(-1/y,1;x\right)\\
&-6G(-1;y)G(-y,0;x) + 12G(-1;y)G(-y,1;x) + 16G(-1,-1,-1;y)\\
&-12G(-1,0,-1;y) - 12G(0,-1,-1;y) + 6G(0,0,-1;y) + 6G(1,0,0;x)\\
&-12G(1,0,1;x) - 12G(1,1,0;x) + 24G(1,1,1;x) - 6G\left(-1/y,0,0;x\right)\\
&+12G\left(-1/y,0,1;x\right) + 6G\left(-1/y,1,0;x\right) - 12G\left(-1/y,1,1;x\right) + 6G(-y,1,0;x)\\
&-12G(-y,1,1;x)\Big]\,.
\end{aligned}
\tag{C.37}
$$

The second MI for the topology Fig. 3-(f) was chosen as follows

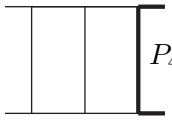

$$
P_4 = \int \frac{\mathfrak{D}^d k_1 \mathfrak{D}^d k_2 \ (k_1-p_1)^2}{P_0(k_1)P_0(k_2)P_0(k_1-k_2)P_0(k_2-p_1)P_0(k_1-p_1-p_2)P_0(k_2-p_1-p_2)P_m(k_1-p_3)}, \tag{C.38}
$$

where

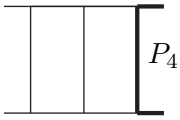

$$
P_4 \quad = \frac{1}{m^4}\sum_{i=-2}^{-1} A_i \varepsilon^i + \mathcal{O}(\varepsilon^0)\,, \tag{C.39}
$$

$$
\begin{aligned}
A_{-2} =& \frac{x^2}{16(1-x)^3(1+x)}\Big[4\zeta(2) + G(0,0;x) - 2G(0,1;x)\Big]\,,\\
A_{-1} =& \frac{x^2}{16(1-x)^3(1+x)}\Big[5\zeta(3) + 24\zeta(2)G(-1;x) - \zeta(2)G(0;x) - 8\ \zeta(2)G(1;x)\\
&-8\zeta(2)G\left(-1/y;x\right) - 4G\left(-1/y;x\right)G(-1,-1;y) + 4G(-y;x)G(-1,-1;y)\\
&+2G(0;x)G(0,-1;y) + 2G\left(-1/y;x\right)G(0,-1;y) - 2G(-y;x)G(0,-1;y)\\
&-2G(-1;y)G\left(-1/y,0;x\right) + 4G(-1;y)G\left(-1/y,1;x\right) + 2G(-1;y)G(-y,0;x)\\
&-4G(-1;y)G(-y,1;x) + 6G(-1,0,0;x) - 12G(-1,0,1;x) + 4G(0,-1,-1;y)\\
&-2G(0,0,-1;y) + 2G(0,0,0;x) - 4G(0,0,1;x) - 6G(0,1,0;x) + 12G(0,1,1;x)\\
&-2G(1,0,0;x) + 4G(1,0,1;x) - 2G\left(-1/y,0,0;x\right) + 4G\left(-1/y,0,1;x\right)\\
&+2G\left(-1/y,1,0;x\right) - 4G\left(-1/y,1,1;x\right) - 2G(-y,1,0;x) + 4G(-y,1,1;x)\Big]\,.
\end{aligned}
\tag{C.40}
$$

The last MI for topology 3-(f) is

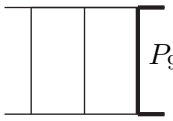

$$= \int \frac{\mathfrak{D}^d k_1 \mathfrak{D}^d k_2 \, \left[(k_2-p_3)^2+m^2\right]}{P_0(k_1) P_0(k_2) P_0(k_1-k_2) P_0(k_2-p_1) P_0(k_1-p_1-p_2) P_0(k_2-p_1-p_2) P_m(k_1-p_3)}, \quad \text{(C.41)}$$

with

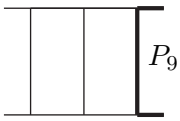

$$= \frac{1}{m^4} \sum_{i=-4}^{-1} A_i \varepsilon^i + \mathcal{O}(\varepsilon^0)\,, \quad \text{(C.42)}$$

$$\begin{aligned}
A_{-4} &= \frac{7x^2}{192(1-x)^4}\,, \\
A_{-3} &= \frac{x^2}{96(1-x)^4}\Big[-8G(-1;y)+3G(0;x)-6G(1;x)\Big]\,, \\
A_{-2} &= \frac{x^2}{24(1-x)^4}\Big[-5\zeta(2)-3G(-1;y)G(0;x)+6G(-1;y)G(1;x)+2G(-1,-1;y)\Big]\,, \\
A_{-1} &= \frac{x^2}{48(1-x)^4}\Big[-29\zeta(3)+58\zeta(2)G(-1;y)+9\zeta(2)G(0;x)+6\zeta(2)\;G(1;x) \\
&\quad -24\zeta(2)G\left(-1/y;x\right)+24G(0;x)G(-1,-1;y)-24G(1;x)G(-1,-1;y) \\
&\quad -12G\left(-1/y;x\right)G(-1,-1;y)-12G(-y;x)G(-1,-1;y)-6G(0;x)G(0,-1;y) \\
&\quad +6G\left(-1/y;x\right)G(0,-1;y)+6G(-y;x)G(0,-1;y)+12G(-1;y)G(1,0;x) \\
&\quad -24G(-1;y)G(1,1;x)-6G(-1;y)G\left(-1/y,0;x\right)+12G(-1;y)G\left(-1/y,1;x\right) \\
&\quad -6G(-1;y)G(-y,0;x)+12G(-1;y)G(-y,1;x)+32G(-1,-1,-1;y) \\
&\quad -12G(-1,0,-1;y)-12G(0,-1,-1;y)+6G(0,0,-1;y)+6G(1,0,0;x) \\
&\quad -12G(1,0,1;x)-12G(1,1,0;x)+24G(1,1,1;x)-6G\left(-1/y,0,0;x\right) \\
&\quad +12G\left(-1/y,0,1;x\right)+6G\left(-1/y,1,0;x\right)-12G\left(-1/y,1,1;x\right)+6G(-y,1,0;x) \\
&\quad -12G(-y,1,1;x)\Big]\,. \qquad \text{(C.43)}
\end{aligned}$$

References

[1] for a recent review see for example W. Bernreuther, J. Phys. G **35**, (2008) 083001 [arXiv:0805.1333].

[2] P. Nason, S. Dawson and R.K. Ellis, Nucl. Phys. B **303** (1988) 607.

[3] P. Nason, S. Dawson and R.K. Ellis, Nucl. Phys. B **327** (1989) 49 [Erratum-ibid. B **335** (1990) 260].

[4] W. Beenakker, H. Kuijf, W.L. van Neerven and J. Smith, Phys. Rev. D **40** (1989) 54.

[5] W. Beenakker, W.L. van Neerven, R. Meng, G.A. Schuler and J. Smith, Nucl. Phys. B **351** (1991) 507.

[6] M.L. Mangano, P. Nason and G. Ridolfi, Nucl. Phys. B **373** (1992) 295.

[7] J.G. Körner and Z. Merebashvili, Phys. Rev. D **66** (2002) 054023 [hep-ph/0207054].

[8] W. Bernreuther, A. Brandenburg, Z.G. Si and P. Uwer, Nucl. Phys. B **690** (2004) 81 [hep-ph/0403035].

[9] M. Czakon and A. Mitov, arXiv:0811.4119.

[10] W. Beenakker, A. Denner, W. Hollik, R. Mertig, T. Sack and D. Wackeroth, Nucl. Phys. B **411** (1994) 343 .

[11] J.H. Kühn, A. Scharf and P. Uwer, Eur. Phys. J. C **45** (2006) 139 [hep-ph/0508092]; Eur. Phys. J. C **51** (2007) 37 [hep-ph/0610335].

[12] W. Bernreuther, M. Fücker and Z.G. Si, Phys. Rev. D **74** (2006) 113005 [hep-ph/0610334]; Phys. Rev. D **78** (2008) 017503 [arXiv:0804.1237].

[13] N. Kidonakis and G. Sterman, Nucl. Phys. B **505** (1997) 321 [hep-ph/9705234].

[14] R. Bonciani, S. Catani, M. L. Mangano and P. Nason, Nucl. Phys. B **529** (1998) 424 [Erratum-ibid. B **803** (2008) 234] [hep-ph/9801375].

[15] M. Cacciari, S. Frixione, M.L. Mangano, P. Nason and G. Ridolfi, JHEP **0404** (2004) 068 [hep-ph/0303085].

[16] S. Moch and P. Uwer, Phys. Rev. D **78** (2008) 034003 [arXiv:0804.1476].

[17] M. Cacciari, S. Frixione, M. L. Mangano, P. Nason and G. Ridolfi, JHEP **0809** (2008) 127 [arXiv:0804.2800].

[18] N. Kidonakis and R. Vogt, Phys. Rev. D **78** (2008) 074005 [arXiv:0805.3844].

[19] M. Czakon and A. Mitov, arXiv:0812.0353.

[20] S. Dittmaier, P. Uwer and S. Weinzierl, Phys. Rev. Lett. **98** (2007) 262002 [hep-ph/0703120]; Eur. Phys. J. C **59** (2009) 625 [arXiv:0810.0452].

[21] J.G. Körner, Z. Merebashvili and M. Rogal, Phys. Rev. D **73** (2006) 034030 [hep-ph/0511264].

[22] J. G. Körner, Z. Merebashvili and M. Rogal, Phys. Rev. D **77** (2008) 094011 [arXiv:0802.0106].

[23] C. Anastasiou and S. M. Aybat, Phys. Rev. D **78** (2008) 114006 [arXiv:0809.1355].

[24] B. Kniehl, Z. Merebashvili, J. G. Korner and M. Rogal, Phys. Rev. D **78** (2008) 094013 [arXiv:0809.3980].

[25] M. Czakon, A. Mitov and S. Moch, Phys. Lett. B **651** (2007) 147 [arXiv:0705.1975].

[26] M. Czakon, A. Mitov and S. Moch, Nucl. Phys. B **798** (2008) 210 [arXiv:0707.4139].

[27] M. Czakon, Phys. Lett. B **664** (2008) 307 [arXiv:0803.1400].

[28] R. Bonciani, A. Ferroglia, T. Gehrmann, D. Maitre and C. Studerus, JHEP **0807** (2008) 129 [arXiv:0806.2301].

[29] S. Laporta and E. Remiddi, Phys. Lett. B **379** (1996) 283 [hep-ph/9602417]; S. Laporta, Int. J. Mod. Phys. A **15** (2000) 5087 [hep-ph/0102033]; F.V. Tkachov, Phys. Lett. B **100** (1981) 65; K.G. Chetyrkin and F.V. Tkachov, Nucl. Phys. B **192** (1981) 159.

[30] A.V. Kotikov, Phys. Lett. B **254** (1991) 158; Phys. Lett. B **259** (1991) 314; Phys. Lett. B **267** (1991) 123; E. Remiddi, Nuovo Cim. A **110** (1997) 1435 [hep-th/9711188]; M. Caffo, H. Czyz, S. Laporta and E. Remiddi, Acta Phys. Polon. B **29** (1998) 2627 [hep-th/9807119]; Nuovo Cim. A **111** (1998) 365 [hep-th/9805118]; T. Gehrmann and E. Remiddi, Nucl. Phys. B **580** (2000) 485 [hep-ph/9912329]; M. Argeri and P. Mastrolia, Int. J. Mod. Phys. A **22** (2007) 4375 [arXiv:0707.4037].

[31] A B. Goncharov, Math. Res. Lett. 5 (1998), 497-516; D.J. Broadhurst, Eur. Phys. J. C **8** (1999) 311 [hep-th/9803091]; E. Remiddi and J.A.M. Vermaseren, Int. J. Mod. Phys. A **15** (2000) 725 [hep-ph/9905237]; T. Gehrmann and E. Remiddi, Comput. Phys. Commun. **141** (2001) 296 [hep-ph/0107173]; D. Maître, Comput. Phys. Commun. **174** (2006) 222 [hep-ph/0507152]; hep-ph/0703052.

[32] J. Vollinga and S. Weinzierl, Comput. Phys. Commun. **167** (2005) 177 [hep-ph/0410259].

[33] T. Gehrmann and E. Remiddi, Nucl. Phys. B **601** (2001) 248 [hep-ph/0008287]; Nucl. Phys. B **601** (2001) 287 [hep-ph/0101124]; Comput. Phys. Commun. **144** (2002) 200 [hep-ph/0111255].

[34] P. Nogueira, J. Comput. Phys. **105** (1993) 279.

[35] J.A.M. Vermaseren, Symbolic Manipulation with `FORM`, Version 2, CAN, Amsterdam, 1991; "New features of FORM" [math-ph/0010025].

[36] M. Argeri, P. Mastrolia and E. Remiddi, Nucl. Phys. B **631** (2002) 388 [hep-ph/0202123].

[37] R. Bonciani, P. Mastrolia and E. Remiddi, Nucl. Phys. B **661** (2003) 289 [Erratum-ibid. B **702** (2004) 359] [hep-ph/0301170]; Nucl. Phys. B **690** (2004) 138 [hep-ph/0311145].

[38] J. Fleischer, A.V. Kotikov and O.L. Veretin, Nucl. Phys. B **547** (1999) 343 [hep-ph/9808242]; U. Aglietti and R. Bonciani, Nucl. Phys. B **668** (2003) 3 [hep-ph/0304028].

[39] A.I. Davydychev and M.Y. Kalmykov, Nucl. Phys. B **699** (2004) 3 [hep-th/0303162].

[40] U. Aglietti and R. Bonciani, Nucl. Phys. B **698** (2004) 277 [hep-ph/0401193].

[41] M. Czakon, J. Gluza and T. Riemann, Phys. Rev. D **71** (2005) 073009 [hep-ph/0412164].

[42] W. Bernreuther, *et al.*, Nucl. Phys. B **706** (2005) 245 [hep-ph/0406046]; Nucl. Phys. B **712** (2005) 229 [hep-ph/0412259]; Nucl. Phys. B **723** (2005) 91 [hep-ph/0504190]; Phys. Rev. D **72** (2005) 096002 [hep-ph/0508254]; Phys. Rev. Lett. **95** (2005) 261802 [hep-ph/0509341]; J. Gluza, A. Mitov, S. Moch and T. Riemann, arXiv:0905.1137.

[43] R. Bonciani, A. Ferroglia, P. Mastrolia, E. Remiddi and J. J. van der Bij, Nucl. Phys. B **681** (2004) 261 [Erratum-ibid. B **702** (2004) 364] [hep-ph/0310333]; R. Bonciani and A. Ferroglia, Phys. Rev. D **72** (2005) 056004 [hep-ph/0507047]; R. Bonciani, A. Ferroglia and A.A. Penin, Phys. Rev. Lett. **100** (2008) 131601 [arXiv:0710.4775]; JHEP **0802** (2008) 080 [arXiv:0802.2215]; S. Actis, M. Czakon, J. Gluza and T. Riemann, Nucl. Phys. B **786** (2007) 26 [arXiv:0704.2400]; Phys. Rev. Lett. **100** (2008) 131602 [arXiv:0711.3847]; Phys. Rev. D **78** (2008) 085019 [arXiv:0807.4691].

[44] R. Bonciani and A. Ferroglia, JHEP **0811** (2008) 065 [arXiv:0809.4687]; H. M. Asatrian, C. Greub and B. D. Pecjak, Phys. Rev. D **78** (2008) 114028 [arXiv:0810.0987]; M. Beneke, T. Huber and X. Q. Li, Nucl. Phys. B **811** (2009) 77 [arXiv:0810.1230]; G. Bell, Nucl. Phys. B **812** (2009) 264 [arXiv:0810.5695].

[45] C. Studerus, to be published.

[46] C. Anastasiou and A. Lazopoulos, JHEP **0407** (2004) 046 [hep-ph/0404258].

[47] V. A. Smirnov, Phys. Lett. B **460** (1999) 397 [hep-ph/9905323]; J. B. Tausk, Phys. Lett. B **469**, 225 (1999) [hep-ph/9909506].

[48] J. Gluza, K. Kajda and T. Riemann, Comput. Phys. Commun. **177** (2007) 879 [arXiv:0704.2423].

[49] M. Czakon, Comput. Phys. Commun. **175** (2006) 559 [hep-ph/0511200].

[50] T. Binoth and G. Heinrich, Nucl. Phys. B **585** (2000) 741 [hep-ph/0004013]; Nucl. Phys. B **693** (2004) 134 [hep-ph/0402265]; G. Heinrich, Nucl. Phys. Proc. Suppl. **116** (2003) 368 [hep-ph/0211144]; Nucl. Phys. Proc. Suppl. **135** (2004) 290 [hep-ph/0406332]; Eur. Phys. J. C **48** (2006) 25 [hep-ph/0601062]; Int. J. Mod. Phys. A **23** (2008) 1457 [arXiv:0803.4177]; A. Gehrmann-De Ridder, T. Gehrmann and G. Heinrich, Nucl. Phys. B **682** (2004) 265 [hep-ph/0311276]; C. Anastasiou, K. Melnikov and F. Petriello, Phys. Rev. D **69** (2004) 076010 [hep-ph/0311311].

[51] A. V. Smirnov and M. N. Tentyukov, Comput. Phys. Commun. **180** (2009) 735 [arXiv:0807.4129].

[52] K. Melnikov and T. van Ritbergen, Nucl. Phys. B **591** (2000) 515 [hep-ph/0005131].

[53] R. Bonciani, A. Ferroglia, T. Gehrmann, and C. Studerus, work in progress.

[54] S. Laporta and E. Remiddi, Nucl. Phys. B **704** (2005) 349 [hep-ph/0406160].

[55] D.A. Kosower, Phys. Rev. D **67** (2003) 116003 [hep-ph/0212097]; A. Daleo, T. Gehrmann and D. Maître, JHEP **0704** (2007) 016 [hep-ph/0612257]; A. Gehrmann-De Ridder and M. Ritzmann, arXiv:0904.3297; A. Gehrmann-De Ridder, T. Gehrmann and E.W.N. Glover, JHEP **0509** (2005) 056 [hep-ph/0505111].

[56] S. Catani and M. Grazzini, Phys. Rev. Lett. **98** (2007) 222002 [hep-ph/0703012].

[57] C. Anastasiou, K. Melnikov and F. Petriello, Phys. Rev. Lett. **93** (2004) 262002 [hep-ph/0409088]; Nucl. Phys. B **724** (2005) 197 [hep-ph/0501130]; JHEP **0709** (2007) 014 [hep-ph/0505069]; K. Melnikov and F. Petriello, Phys. Rev. Lett. **96** (2006) 231803 [hep-ph/0603182]; Phys. Rev. D **74** (2006) 114017 [hep-ph/0609070]; C. Anastasiou, G. Dissertori and F. Stöckli, JHEP **0709** (2007) 018 [arXiv:0707.2373].

[58] M. Grazzini, JHEP **0802** (2008) 043 [arXiv:0801.3232]; D. de Florian and M. Grazzini, Phys. Lett. B **674** (2009) 291 [arXiv:0901.2427]; S. Catani, L. Cieri, G. Ferrera, D. de Florian and M. Grazzini, arXiv:0903.2120.

[59] A. Gehrmann-De Ridder, T. Gehrmann, E.W.N. Glover and G. Heinrich, Phys. Rev. Lett. **99** (2007) 132002 [arXiv:0707.1285]; JHEP **0711** (2007) 058 [arXiv:0710.0346]; JHEP **0712** (2007) 094 [arXiv:0711.4711]; Phys. Rev. Lett. **100** (2008) 172001 [arXiv:0802.0813]; JHEP **0905** (2009) 106 [arXiv:0903.4658].

[60] S. Weinzierl, Phys. Rev. Lett. **101** (2008) 162001 [arXiv:0807.3241]; JHEP **0906** (2009) 041 [arXiv:0904.1077]; arXiv:0904.1145.